Strathclyde Engagement with the National HVDC Centre: Phase 2 Assessment and Mitigation of Converter Interactions

Doc. Type:	Technical Report	*Date:* **2/10/2019**	
Doc. Nº:	**USTRATH-HVDC Centre-P2-001**	*Issue: 1*	*Page:* **1** *of* **37**
Title:	Development and Validation of MMC Converter Impedance Models		

	Name&Function	*Signature*	*Date*
Prepared by:	Deyang Guo, Yin Chen, Agusti Egea, Gabriele Amico, University of Strathclyde	Deyang Guo Yin Chen Gabriele Amico	30/08/2019
Approved by:	Lie Xu, University of Strathclyde		02/10/2019
Authorized by:	Ben Marshall, The National HVDC Centre		03/07/2020
Accepted by:	Simon Marshall, The National HVDC Centre		03/07/2020

DISTRIBUTION LIST	N	A	I
Internal			
External			

N=Number of copy
A=Application
I=Information

TABLE OF CONTENT

Executive summary

This document describes the work carried out as part of the joint Strathclyde-UK National HVDC Centre project "Assessment and Mitigation of Converter Interactions". This report covers the first task of the project on the development and RTDS validation of impedance-based HVDC system models. This task develops and validates impedance-based MMC small signal models that can be used for assessing stability and interactions between converters in the later tasks.

Conventional small signal converter modelling methods consider the same frequency component for the state variables, and the inputs and outputs, i.e. an input at one specific frequency will only generate an output at the same frequency. However, the existence of significant steady-state harmonic components in the arm currents and capacitor voltages of MMC converters, it is necessary to consider the MMC internal dynamics and harmonic interaction in the small-signal modelling for stability assessment. Thus, the conventional modelling methods become unsuitable and in this task, an impedance-based MMCs small-signal model using harmonic state space (HSS) modelling has been developed making use of the latest modelling techniques described in the literature and new developments initiated by the Strathclyde team. The HSS modelling simultaneously represents multiple frequency responses in each variable and leads to multidimensional harmonic transfer function based models. The developed HSS models contain harmonics of state variables, inputs, and outputs posed separately in a state-space form so can be easily implemented by computing programs (e.g., MATLAB) and extended to any number of harmonics.

To validate the developed MMCs small signal models, frequency injection/sweep method in time domain models in Simulink/PSCAD/RTDS simulation platforms are used considering different system configurations, including:

- the converter small-signal impedance (open loop with electrical components only) has been obtained and validated against Simulink, PSCAD and RTDS models;
- the converter small-signal impedance including circulating current controller has been obtained and validated against Simulink, PSCAD and RTDS models;
- the converter small-signal impedance including circulating current controller and AC current controller in the dq-frame has been obtained and validated against Simulink and PSCAD;

This developed analytical model will be used for assessing stability and interactions between converters operating in close vicinity in the following phases of the project where multiple converters and representative AC network models will be combined for stability assessment.

1 General introduction

The rapid growth in the amount of converter-interfaced renewable sources and HVDC transmission links is significantly changing the characteristics of the GB grid. The wide timescale control dynamics of converters located in close vicinities can result in coupled effects among the converters and power networks, and can lead to oscillations across a wide frequency range. Accurate assessment of potential system interactions is critical for ensuring stable operation of future and evolving GB network. The report describes the development of accurate small signal frequency domain models of MMC converters for stability analysis.

To assess the stability of grid connected converter systems, traditional approaches use converter control models that account for the grid and the coupling with other grid-connected converters [1]. However, such approaches require detailed converter control models and their loop stability analysis are necessary for the design of individual converters. When the objective is grid system stability analysis, external behaviour of a converter is of more interest than its internal loop stability and is also easier to obtain. In such cases, the impedance-based approach is more advantageous and effective, as it avoids the need to remodel each inverter and repeat its loop stability analysis when the grid changes, or when more inverters are connected to the same grid [2].

Conventional small signal modelling methods consider the same frequency component for the state variables, the inputs and the outputs, indicating that a specific frequency input will only generate an output at the same frequency. However, the existence of significant steady-state harmonic components in the arm currents and capacitor voltages of MMC converters, it is necessary to consider the MMC internal dynamics and harmonic interaction in the small-signal modelling for stability assessment [3]. This means that an input at one frequency will generate outputs at multiples frequencies (called harmonics here). Thus, the conventional modelling methods become unsuitable and harmonic state space (HSS) modelling technique which considers multi-harmonic interactions is used to develop the analytical MMC models. The HSS modelling simultaneously represents multiple frequency responses in each variable and leads to multidimensional harmonic transfer function based models.

To validate the developed analytical models, step-by-step validation processes using time-domain simulation models in multiple simulation platforms, e.g. Simulink, PSCAD and RSCAD are carried out using frequency sweep method.

The rest of the report is organised as follows. Chapter 2 describes the basis of the method to study stability using converter and grid impedance, and introduces the method to calculate the impedance. Chapter 3 presents the method to linearize the MMC using the HSS representation and the validation of the converter open-loop impedance. Chapter 4 introduces the impedance modelling of the MMC considering the circulating current controller and AC current control in the dq-frame.

2 Introduction to impedance-based converter modelling and stability assessment

2.1 Background

Power converter small-signal stability assessment usually involves complicated models where all the converter states are represented. These models are usually defined in the dq-frame (as current controller is usually implemented in the dq frame) and require detailed knowledge of the control structure. As the converter controller is a sensitive part of the converter system and is usually subject to IP, therefore, it is very difficult for HVDC link or wind farm owners or systems operators to have them. On the other hand, when the objective is grid system stability analysis, external behaviour of a converter is of more interest than its internal loop stability. In such cases, the impedance-based approach is more advantageous and effective, as it avoids the need to remodel each inverter and the impedance can be obtained using the converter control mathematical model or using real power converter measurements.

2.2 Principals of impedance-based stability assessment

As a simplified grid connected converter system as shown in Figure 1(a), the impedance stability assessment approach requires a representation of the converter and the grid small-signal model in terms of electrical impedances. The converter is modelled as a controlled current source and is therefore represented by its Norton equivalent as shown in Figure 1 (b), while the grid is described in terms of its Thevenin equivalent. Z_c is the output small-signal admittance of the inverter and includes the line reactor connected in series to its AC terminals (Z_f in Figure 1(a)). It allows quantifying the effect of the converter controller on the measured voltage U and current i signals. The grid is modelled using a Thevenin grid equivalent or more complex model Z_{TH}

Once both impedances are obtained it is possible to study the stability applying standard control techniques considering that the converter admittance ($Y_c=1/Z_c$) is connected in series with the grid impedance Z_{TH}. This procedure will be detailed in Task 3 in future reports.

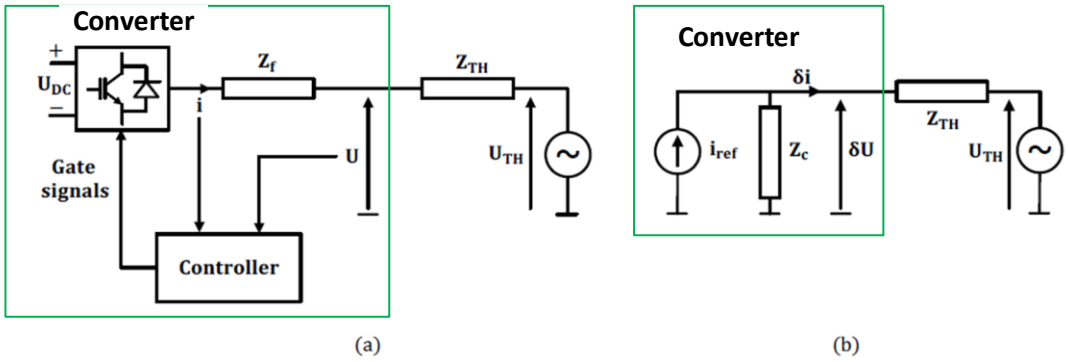

Figure 1: a) Scheme of a grid-connected power converter b) Impedance representation of the grid-connected converter.

The small-signal converter admittance is calculated based on the small-signal model of the converter controller, whose dynamics are linearised at an operating point. This admittance also includes the coupling reactor interfacing the inverter to the rest of the electrical system. The small-signal converter admittance is defined as the transfer function $Y_C(s)$ from the small-signal voltage U(s) to the small-signal inverter current i(s) (see Figure 2 where U_0 and i_0 represent the steady-state values of U and i, at the system operating point):

$$Y_C(s) = -\frac{\delta i(s)}{\delta U(s)} \tag{1}$$

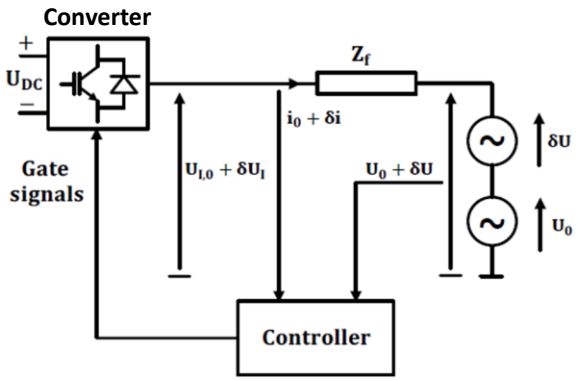

Figure 2: Calculation of the converter small-signal impedance

This impedance can be calculated in multiple references frames (Figure 3). Depending on the study, different reference frames can be used, usually the dq-frame or αβ-frame are the preferred frames for control designs, whereas abc-frame is the natural impedance frame. Recently some studies have highlighted that the pn-frame (i.e. positive and negative sequence frame) might have some interest in stability studies. The impedances expressed in one reference frame can be translated to another frame applying different transformations abc-frame to dq-frame (Park transformation), abc-frame to pn-frame. In the following section, an example from the translation of an impedance from abc-frame to dq-frame is presented.

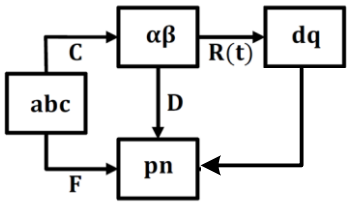

Figure 3: Different reference frames to express three-phase electrical systems

2.3 Translation of a transfer function from the abc- to the positive dq-frame

In this section, the relation between the transfer function matrix $G_M(s)$ defined in the abc-frame and its equivalent expression in the dq-frame is derived. The particular case where $G_M(s)$ has the structure defined in (2) is considered, where $G(s)$ is a generic transfer function.

$$\begin{bmatrix} y_a(s) \\ y_b(s) \\ y_c(s) \end{bmatrix} = G_M(s) \begin{bmatrix} x_a(s) \\ x_b(s) \\ x_c(s) \end{bmatrix} = \begin{bmatrix} G(s) & 0 & 0 \\ 0 & G(s) & 0 \\ 0 & 0 & G(s) \end{bmatrix} \begin{bmatrix} x_a(s) \\ x_b(s) \\ x_c(s) \end{bmatrix} \tag{2}$$

The signals $y_{abc}(s)$ and $x_{abc}(s)$ are the Laplace transform of the corresponding time-domain signals $y_{abc}(t)$ and $x_{abc}(t)$, respectively. In other words $x_{abc}(s) = L\{x_{abc}(t)\}$ and $y_{abc}(s) = L\{y_{abc}(t)\}$. By applying the Park transform $T(\omega_0 t)$ (3) and its transpose $T^T(\omega_0 t)$ (4), such time-domain signals can be related to their dq-frame counterparts, $y_{dq}(t)$ and $x_{dq}(t)$ respectively, as depicted by (5).

$$\begin{bmatrix} f_d(t) \\ f_q(t) \end{bmatrix} = T(\theta(t)) \begin{bmatrix} f_a(t) \\ f_b(t) \\ f_c(t) \end{bmatrix} = \frac{2}{3} \cdot \begin{bmatrix} sin(\theta(t)) & sin(\theta(t) - \frac{2}{3}\pi) & sin(\theta(t) - \frac{4}{3}\pi) \\ cos(\theta(t)) & cos(\theta(t) - \frac{2}{3}\pi) & cos(\theta(t) - \frac{4}{3}\pi) \end{bmatrix} \begin{bmatrix} f_a(t) \\ f_b(t) \\ f_c(t) \end{bmatrix} \tag{3}$$

$$\begin{bmatrix} f_a(t) \\ f_b(t) \\ f_c(t) \end{bmatrix} = T^T(\theta(t)) \begin{bmatrix} x_d(t) \\ x_q(t) \end{bmatrix} = \begin{bmatrix} sin(\theta(t)) & cos(\theta(t)) \\ sin(\theta(t) - \frac{2}{3}\pi) & cos(\theta(t) - \frac{2}{3}\pi) \\ sin(\theta(t) - \frac{4}{3}\pi) & cos(\theta(t) - \frac{4}{3}\pi) \end{bmatrix} \begin{bmatrix} f_d(t) \\ f_q(t) \end{bmatrix} \tag{4}$$

$$\begin{bmatrix} x_d(t) \\ x_q(t) \end{bmatrix} = \frac{2}{3} \cdot \begin{bmatrix} sin(\omega_0 t) & sin(\omega_0 t - \frac{2}{3}\pi) & sin(\omega_0 t - \frac{4}{3}\pi) \\ cos(\omega_0 t) & cos(\omega_0 t - \frac{2}{3}\pi) & cos(\omega_0 t - \frac{4}{3}\pi) \end{bmatrix} \begin{bmatrix} x_a(t) \\ x_b(t) \\ x_c(t) \end{bmatrix}$$

$$\begin{bmatrix} y_d(t) \\ y_q(t) \end{bmatrix} = \frac{2}{3} \cdot \begin{bmatrix} sin(\omega_0 t) & sin(\omega_0 t - \frac{2}{3}\pi) & sin(\omega_0 t - \frac{4}{3}\pi) \\ cos(\omega_0 t) & cos(\omega_0 t - \frac{2}{3}\pi) & cos(\omega_0 t - \frac{4}{3}\pi) \end{bmatrix} \begin{bmatrix} y_a(t) \\ y_b(t) \\ y_c(t) \end{bmatrix}$$

$$\begin{bmatrix} x_a(t) \\ x_b(t) \\ x_c(t) \end{bmatrix} = \begin{bmatrix} sin(\omega_0 t)) & cos(\omega_0 t) \\ sin(\omega_0 t - \frac{2}{3}\pi) & cos(\omega_0 t - \frac{2}{3}\pi) \\ sin(\omega_0 t - \frac{4}{3}\pi) & cos(\omega_0 t - \frac{4}{3}\pi) \end{bmatrix} \begin{bmatrix} x_d(t) \\ x_q(t) \end{bmatrix} \tag{5}$$

$$\begin{bmatrix} y_a(t) \\ y_b(t) \\ y_c(t) \end{bmatrix} = \begin{bmatrix} sin(\omega_0 t)) & cos(\omega_0 t) \\ sin(\omega_0 t - \frac{2}{3}\pi) & cos(\omega_0 t - \frac{2}{3}\pi) \\ sin(\omega_0 t - \frac{4}{3}\pi) & cos(\omega_0 t - \frac{4}{3}\pi) \end{bmatrix} \begin{bmatrix} y_d(t) \\ y_q(t) \end{bmatrix}$$

From (5), by making use of Euler's formula, the following equations (6) and (7) can be derived for $y_{dq}(t)$ and $x_{abc}(t)$, respectively:

$$\begin{aligned}
y_d(t) &= \frac{2}{3}[sin(\omega_0 t)y_a(t) + sin(\omega_0 t - \frac{2}{3}\pi)y_b(t) + sin(\omega_0 t - \frac{4}{3}\pi)y_c(t)] \\
&= \frac{1}{3j}[(e^{j\omega_0 t} - e^{-j\omega_0 t})y_a(t) + (e^{j(\omega_0 t - \frac{2}{3}\pi)} - e^{-j(\omega_0 t - \frac{2}{3}\pi)})y_b(t) \\
&+ (e^{j(\omega_0 t - \frac{4}{3}\pi)} - e^{-j(\omega_0 t - \frac{4}{3}\pi)})y_c(t)] \\
y_q(t) &= \frac{2}{3}[cos(\omega_0 t)y_a(t) + cos(\omega_0 t - \frac{2}{3}\pi)y_b(t) + cos(\omega_0 t - \frac{4}{3}\pi)y_c(t)] \\
&= \frac{1}{3}[(e^{j\omega_0 t} + e^{-j\omega_0 t})y_a(t) + (e^{j(\omega_0 t - \frac{2}{3}\pi)} + e^{-j(\omega_0 t - \frac{2}{3}\pi)})y_b(t) \\
&+ (e^{j(\omega_0 t - \frac{4}{3}\pi)} + e^{-j(\omega_0 t - \frac{4}{3}\pi)})y_c(t)]
\end{aligned} \tag{6}$$

$$\begin{aligned}
x_a(t) &= sin(\omega_0 t)x_d(t) + cos(\omega_0 t)x_q(t) \\
&= \frac{1}{2j}(e^{j\omega_0 t} - e^{-j\omega_0 t})x_d(t) + \frac{1}{2}(e^{j\omega_0 t} + e^{-j\omega_0 t})x_q(t) \\
x_b(t) &= sin(\omega_0 t - \frac{2}{3}\pi)x_d(t) + cos(\omega_0 t - \frac{2}{3}\pi)x_q(t) \\
&= \frac{1}{2j}(e^{j(\omega_0 t - \frac{2}{3}\pi)} - e^{-j(\omega_0 t - \frac{2}{3}\pi)})x_d(t) + \frac{1}{2}(e^{j(\omega_0 t - \frac{2}{3}\pi)} + e^{-j(\omega_0 t - \frac{2}{3}\pi)})x_q(t) \\
x_c(t) &= sin(\omega_0 t - \frac{4}{3}\pi)x_d(t) + cos(\omega_0 t - \frac{4}{3}\pi)x_q(t) \\
&= \frac{1}{2j}(e^{j(\omega_0 t - \frac{4}{3}\pi)} - e^{-j(\omega_0 t - \frac{4}{3}\pi)})x_d(t) + \frac{1}{2}(e^{j(\omega_0 t - \frac{4}{3}\pi)} + e^{-j(\omega_0 t - \frac{4}{3}\pi)})x_q(t)
\end{aligned} \tag{7}$$

The corresponding Laplace transform signals of (6), (7) are:

$$\begin{aligned}
y_d(s) &= \frac{1}{3j}[y_a(s - j\omega_0) - y_a(s + j\omega_0) + y_b(s - j\omega_0)e^{-j\frac{2}{3}\pi} - y_b(s + j\omega_0)e^{j\frac{2}{3}\pi} \\
&+ y_c(s - j\omega_0)e^{-j\frac{4}{3}\pi} - y_c(s + j\omega_0)e^{j\frac{4}{3}\pi}] \\
y_q(s) &= \frac{1}{3}[y_a(s - j\omega_0) + y_a(s + j\omega_0) + y_b(s - j\omega_0)e^{-j\frac{2}{3}\pi} + y_b(s + j\omega_0)e^{j\frac{2}{3}\pi} \\
&+ y_c(s - j\omega_0)e^{-j\frac{4}{3}\pi} + y_c(s + j\omega_0)e^{j\frac{4}{3}\pi}]
\end{aligned} \tag{8}$$

$$\begin{aligned}
x_a(s) &= \frac{1}{2}[-jx_d(s - j\omega_0) + x_d(s + j\omega_0) + x_q(s - j\omega_0) + x_q(s + j\omega_0)] \\
x_b(s) &= \frac{1}{2}[-jx_d(s - j\omega_0)e^{-j\frac{2}{3}\pi} + x_d(s + j\omega_0)e^{j\frac{2}{3}\pi} + x_q(s - j\omega_0)e^{-j\frac{2}{3}\pi} + x_q(s + j\omega_0)e^{j\frac{2}{3}\pi}] \\
x_c(s) &= \frac{1}{2}[-jx_d(s - j\omega_0)e^{-j\frac{4}{3}\pi} + x_d(s + j\omega_0)e^{j\frac{4}{3}\pi} + x_q(s - j\omega_0)e^{-j\frac{4}{3}\pi} + x_q(s + j\omega_0)e^{j\frac{4}{3}\pi}]
\end{aligned} \tag{9}$$

Thereby, as from (2), $y_a(s) = G(s)x_a(s)$, $y_b(s) = G(s)x_b(s)$ and $y_c(s) = G(s)x_c(s)$, replacing the expression of $x_{abc}(s)$ given by (9) in the expression of $y_{dq}(s)$ provided by (8), the following equations can be derived:

$$\begin{aligned} y_d(s) &= \frac{1}{2}[G(s-j\omega_0)+G(s+j\omega_0)]x_d(s) + \frac{1}{2}j[G(s+j\omega_0)-G(s-j\omega_0)]x_q(s) \\ y_q(s) &= \frac{1}{2}j[G(s-j\omega_0)-G(s+j\omega_0)]x_d(s) + \frac{1}{2}[G(s-j\omega_0)+G(s+j\omega_0)]x_q(s) \end{aligned} \tag{10}$$

These can be reformulated in a matrix format as:

$$\begin{bmatrix} y_d(s) \\ y_q(s) \end{bmatrix} = \begin{bmatrix} \frac{1}{2}[G(s-j\omega)+G(s+j\omega)] & \frac{1}{2}j[G(s+j\omega_0)-G(s-j\omega_0)] \\ \frac{1}{2}j[G(s-j\omega_0)-G(s+j\omega_0)] & \frac{1}{2}[G(s-j\omega_0)+G(s+j\omega_0)] \end{bmatrix} \begin{bmatrix} x_d(s) \\ x_q(s) \end{bmatrix} \tag{11}$$

The matrix $G_{M,DQ}(s)$ is defined as:

$$G_{M,DQ}(s) = \begin{bmatrix} \frac{1}{2}[G(s-j\omega)+G(s+j\omega)] & \frac{1}{2}j[G(s+j\omega_0)-G(s-j\omega_0)] \\ \frac{1}{2}j[G(s-j\omega_0)-G(s+j\omega_0)] & \frac{1}{2}[G(s-j\omega_0)+G(s+j\omega_0)] \end{bmatrix} \tag{12}$$

Therefore, equation (12) represents the expression of the abc-frame matrix $G_M(s)$ in the dq-frame.

2.4 Limitations of Small-signal Impedance modelling techniques

The small-signal modelling of the converter is a compact form to get the converter and the grid dynamics but compared to other small-signal models might not provide enough information to identify the parts of the controller that might be unstable. More detailed discussion will be provided in Task 3 deliverables when system stability is assessed. In addition, as for any small signal models, they cannot be used to assess dynamic system response during large transients.

3 MMC Small-signal impedance modelling

3.1 HSS modelling

The harmonic state space (HSS) modelling method was originally developed in [1] for the purpose of modelling vibrations of helicopter blades, which exhibit periodic dynamics. The basic idea of HSS is to derive a linear time-invariant representation of the linear time-periodic system, and thus the linear control theory can be used for the stability analysis and controller design. The HSS modelling method is able to represent multiple frequency responses in each variable and build multidimensional harmonic transfer function based models. It is introduced in modelling MMC system in order to include internal dynamics of the converter in [1].

For any time-varying periodic signal $x(t)$, it can be expressed as the Fourier series, i.e.

$$x(t) = \sum_{k\in Z} X_k e^{jk\omega_1 t} \tag{13}$$

where X_k is the Fourier coefficient and is calculated as

$$X_k = \frac{1}{T}\int_{t_0}^{t_0+T} x(t)e^{-jk\omega_1 t}dt \tag{14}$$

In (14), T and ω_1 are the fundamental period and frequency of the signal, respectively and are governed by $\omega_1 = 2\pi/T$. The time-domain state-space equation of the MMC system can be expressed as

$$\dot{x}(t) = A(t)x(t) + B(t)u(t) \tag{15}$$

Based on the harmonic balance theory [1], the time-domain state-space equation of the studied system (15) is transformed into the frequency-domain HSS equation

$$s\mathbb{X} = (\mathbb{A} - \mathbb{Q})\mathbb{X} + \mathbb{B}\mathbb{U} \tag{16}$$

where the variables of $\mathbb{X}$, $\mathbb{U}$, $\mathbb{A}$, $\mathbb{B}$, and $\mathbb{Q}$ are expressed as (17)-(21) in which the elements X_h, U_h, A_h, B_h are the corresponding h-th Fourier coefficients of $X(t), U(t), A(t)$ and $B(t)$, respectively.

$$\mathbb{X} = [X_{-h}, \dots, X_{-1}, X_0, X_1, \dots, X_h]^T \tag{17}$$

$$\mathbb{U} = [U_{-h}, \dots, U_{-1}, U_0, U_1, \dots, U_h]^T \tag{18}$$

$$\mathbb{A} = \begin{bmatrix} A_0 & A_{-1} & \dots & A_{-h} & & & \\ A_1 & \ddots & \ddots & \ddots & \ddots & & \\ \vdots & \ddots & A_0 & A_{-1} & \ddots & \ddots & \\ A_h & \ddots & A_1 & A_0 & A_{-1} & \ddots & A_{-h} \\ & \ddots & \ddots & A_1 & A_0 & \ddots & \vdots \\ & & \ddots & \ddots & \ddots & \ddots & A_{-1} \\ & & & A_h & \dots & A_1 & A_0 \end{bmatrix} \tag{19}$$

$$\mathbb{B} = \begin{bmatrix} B_0 & B_{-1} & \dots & B_{-h} & & & \\ B_1 & \ddots & \ddots & \ddots & \ddots & & \\ \vdots & \ddots & B_0 & B_{-1} & \ddots & \ddots & \\ B_h & \ddots & B_1 & B_0 & B_{-1} & \ddots & B_{-h} \\ & \ddots & \ddots & B_1 & B_0 & \ddots & \vdots \\ & & \ddots & \ddots & \ddots & \ddots & B_{-1} \\ & & & B_h & \dots & B_1 & B_0 \end{bmatrix} \tag{20}$$

$$\mathbb{Q} = \begin{bmatrix} -jh\omega_1 \cdot I & & & & \\ & \ddots & & & \\ & & 0 \cdot I & & \\ & & & \ddots & \\ & & & & jh\omega_1 \cdot I \end{bmatrix} \tag{21}$$

3.2 Impedance based modelling procedure

3.2.1 HSS-based large-signal model of MMC

Figure 4 shows the circuit diagram of one phase of a three-phase MMC converter. The average-value modelling method is used which means it is assumed that the capacitor voltages are balanced at all time. A lumped capacitor is used to mimic the dynamic of each arm [5]. In addition, an AC load of $Z_L (= R_{load} + j\omega_1 L_{load})$ is considered on the output to determine the steady-state operating point.

According to Kirchhoff's law, the dynamics of the upper and lower arms of the single-phase MMC as shown in Figure 4 are expressed as:

$$v_g(t) + L\frac{di_u(t)}{dt} + Ri_u(t) + v_u(t) = \frac{V_{dc}}{2} \tag{22}$$

$$v_g(t) - L\frac{di_l(t)}{dt} - Ri_l(t) - v_l(t) = -\frac{V_{dc}}{2} \tag{23}$$

According to the averaged model of the MMC, internal dynamics of the single-phase are expressed as:

$$C_{arm}\frac{dv_{cu}^{\Sigma}(t)}{dt} = n_u(t)i_u(t) \tag{24}$$

$$C_{arm}\frac{dv_{cl}^{\Sigma}(t)}{dt} = n_l(t)i_l(t) \tag{25}$$

$$v_u(t) = n_u(t)v_{cu}^{\Sigma} \tag{26}$$

$$v_l(t) = n_l(t)v_{cl}^{\Sigma} \tag{27}$$

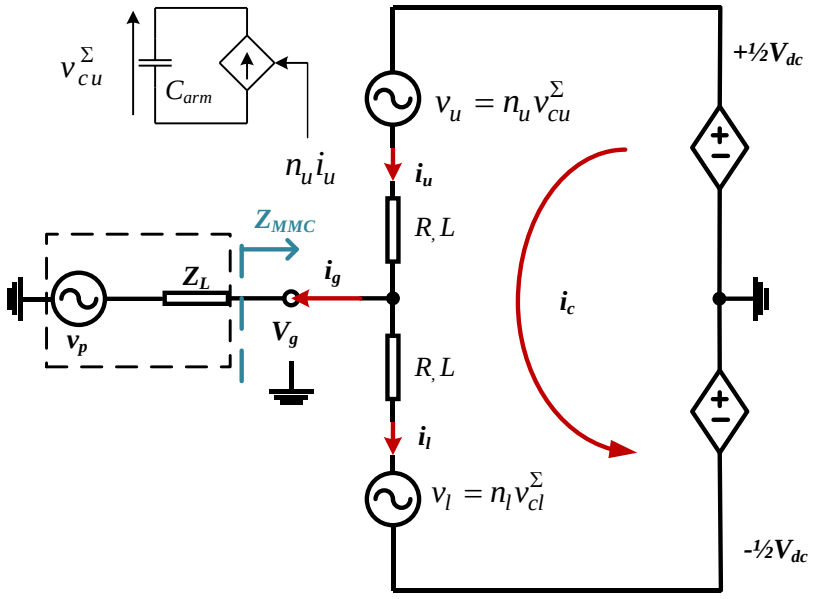

Figure 4: Single-line diagram of the average value model of the MMC

The AC-side current $i_g(t)$ and the circulating current $i_c(t)$ are defined as:

$$i_c(t) = \frac{i_u(t) + i_l(t)}{2} \tag{28}$$

$$i_g(t) = i_u(t) - i_l(t) \tag{29}$$

Equations (22)-(29) represent the dynamics of the power stage of the MMC. Rewriting (22)-(29) in the matrix form yields:

$$x(t) = \left[i_c(t), v_{cu}^{\Sigma}(t), v_{cl}^{\Sigma}(t), i_g(t)\right]^T \tag{30}$$

$$u(t) = [V_{dc}] \tag{31}$$

$$A(t) = \begin{bmatrix} -\frac{R}{L} & -\frac{n_u(t)}{2L} & -\frac{n_l(t)}{2L} & 0 \\ \frac{n_u(t)}{C_{arm}} & 0 & 0 & \frac{n_u(t)}{2C_{arm}} \\ \frac{n_l(t)}{C_{arm}} & 0 & 0 & -\frac{n_l(t)}{2C_{arm}} \\ 0 & -\frac{n_u(t)}{L} & -\frac{n_l(t)}{L} & -\frac{R+2Z_L}{L} \end{bmatrix} \quad (32)$$

$$B(t) = \left[\frac{1}{2L}, 0, 0, 0\right]^T \quad (33)$$

In this section, the HSS model of MMC with open-loop control is developed and thus the switching functions for upper and lower arms of the single-phase model are defined as (34) and (35), respectively:

$$n_u(t) = \frac{1}{2}[1 - m_1\cos(\omega_1 t + \theta_{m1}) - m_2\cos(2\omega_1 t + \theta_{m2}) + \sum_{n=3}^{\infty} m_n\cos(n\omega_1 t + \theta_{mn})] \quad (34)$$

$$n_l(t) = \frac{1}{2}\left[1 + m_1\cos(\omega_1 t + \theta_{m1}) - m_2\cos(2\omega_1 t + \theta_{m2}) + \sum_{n=3}^{\infty} m_n\cos(n\omega_1 t + \theta_{mn})\right] \quad (35)$$

where m and θ_{m1} are the fundamental modulation index and phase angle generated by the fundamental controller, m_2 and θ_{m2} are the second-order harmonic modulation index and phase angle generated by the second-order harmonic circulating current controller. In MMC control system, the harmonic components of modulation voltage above second order are usually very small and can be neglected, i.e. $m_n = 0 \quad (n \geq 3)$.

Following the HSS modelling method described in Section 3.1, the time-domain state-space model of the MMC formulated as (15) and (30)-(33) can be converted into the HSS model, as expressed by (16). As upper and lower switching functions $n_u(t)$ and $n_l(t)$ contain significant steady-state harmonic components, the Euler's formula is applied to (34) and (35) to calculate the Fourier coefficient of elements in $A(t)$, expressed as (36) and (37) as:

$$n_u(t) = \frac{1}{2}\left[1 - \frac{m_1}{2}\left(e^{j\omega_1 t + j\theta_{m1}} + e^{-j\omega_1 t - j\theta_{m1}}\right) - \frac{m_2}{2}\left(e^{j2\omega_1 t + j\theta_{m2}} + e^{-j2\omega_1 t - j\theta_{m2}}\right)\right] \quad (36)$$

$$n_l(t) = \frac{1}{2}\left[1 + \frac{m_1}{2}\left(e^{j\omega_1 t + j\theta_{m1}} + e^{-j\omega_1 t - j\theta_{m1}}\right) - \frac{m_2}{2}\left(e^{j2\omega_1 t + j\theta_{m2}} + e^{-j2\omega_1 t - j\theta_{m2}}\right)\right] \quad (37)$$

The matrixes X (X_0, $X_{\pm1}$, $X_{\pm2}\ldots$ and $X_{\pm h}$), U (U_0, $U_{\pm1}$, $U_{\pm2}\ldots$ and $U_{\pm h}$), A (A_0, $A_{\pm1}$, $A_{\pm2}\ldots$ and $A_{\pm h}$) and B (B_0, $B_{\pm1}$, $B_{\pm2}\ldots$ and $B_{\pm h}$) are depicted as (38)-(46), respectively, where the matrix elements are derived by calculating the Fourier coefficient of corresponding element in $A(t)$ as shown in (32).

$$X_{\pm h} = \left[I_{c\pm h}, V^{\Sigma}_{cu\pm h}, V^{\Sigma}_{cl\pm h}, I_{g\pm h}\right] \tag{38}$$

$$U_0 = [V_{dc}] \tag{39}$$

$$U_{\pm h} = [0], (h \geq 1) \tag{40}$$

$$A_0 = \begin{bmatrix} -\frac{R}{L} & -\frac{1}{4L} & -\frac{1}{4L} & 0 \\ \frac{1}{2C_{arm}} & 0 & 0 & \frac{1}{4C_{arm}} \\ \frac{1}{2C_{arm}} & 0 & 0 & -\frac{1}{4C_{arm}} \\ 0 & -\frac{1}{2L} & -\frac{1}{2L} & -\frac{R+2Z_L}{L} \end{bmatrix} \tag{41}$$

$$A_{\pm1} = \begin{bmatrix} 0 & \frac{m_1 e^{\pm j\theta_{m1}}}{8L} & -\frac{m_1 e^{\pm j\theta_{m1}}}{8L} & 0 \\ -\frac{m_1 e^{\pm j\theta_{m1}}}{4C_{arm}} & 0 & 0 & -\frac{m_1 e^{\pm j\theta_{m1}}}{8C_{arm}} \\ \frac{m_1 e^{\pm j\theta_{m1}}}{4C_{arm}} & 0 & 0 & -\frac{m_1 e^{\pm j\theta_{m1}}}{8C_{arm}} \\ 0 & \frac{m_1 e^{\pm j\theta_{m1}}}{4C_{arm}} & \frac{m_1 e^{\pm j\theta_{m1}}}{4C_{arm}} & 0 \end{bmatrix} \tag{42}$$

$$A_{\pm2} = \begin{bmatrix} 0 & \frac{m_2 e^{\pm j\theta_{m2}}}{8L} & \frac{m_2 e^{\pm j\theta_{m2}}}{8L} & 0 \\ -\frac{m_2 e^{\pm j\theta_{m1}}}{4C_{arm}} & 0 & 0 & -\frac{m_2 e^{\pm j\theta_{m2}}}{8C_{arm}} \\ -\frac{m_2 e^{\pm j\theta_{m1}}}{4C_{arm}} & 0 & 0 & \frac{m_2 e^{\pm j\theta_{m2}}}{8C_{arm}} \\ 0 & \frac{m_2 e^{\pm j\theta_{m2}}}{4C_{arm}} & -\frac{m_2 e^{\pm j\theta_{m2}}}{4C_{arm}} & 0 \end{bmatrix} \tag{43}$$

$$A_{\pm h} = \begin{bmatrix} 0 & 0 & 0 & 0 \\ 0 & 0 & 0 & 0 \\ 0 & 0 & 0 & 0 \\ 0 & 0 & 0 & 0 \end{bmatrix}, (h \geq 3) \tag{44}$$

$$B_0 = \left[\frac{1}{2L}, 0,0,0\right]^T \tag{45}$$

$$B_{\pm h} = [0,0,0,0]^T, (h \geq 1) \tag{46}$$

Assuming the left side of (16) is zero, the steady-state harmonics of state variables is calculated as

$$\mathbb{X}_{SS} = -(\mathbb{A} - \mathbb{Q})^{-1}(\mathbb{B}\mathbb{U}) \tag{47}$$

3.2.2 HSS-based small-signal model of MMC

All the state variables in equations (22)-(35) are periodic signals in the steady state, and the MMC is essentially a nonlinear time periodic (NTP) system. Based on the HSS modelling method, the small-signal linear time periodic (LTP) equations of the MMC is obtained by linearizing (22)-(35) around operating points as:

$$\begin{aligned} \frac{d\Delta i_c(t)}{dt} &= -\frac{R}{L}\Delta i_c(t) - \frac{1}{2L}\Delta v_u(t) - \frac{1}{2L}\Delta v_l(t) \\ &= -\frac{R}{L}\Delta i_c(t) - \frac{1}{2L}\left(\Delta n_u(t) v_{cu0}^{\Sigma} + n_{u0}(t)\Delta v_{cu}^{\Sigma} + \Delta n_l(t) v_{cl0}^{\Sigma} + n_{l0}(t)\Delta v_{cl}^{\Sigma}\right) \end{aligned} \tag{48}$$

$$\begin{aligned} \frac{d\Delta i_g(t)}{dt} &= -\frac{R}{L}\Delta i_g(t) - \frac{1}{L}\Delta v_{u}(t) + \frac{1}{L}\Delta v_{l}(t) - \frac{2}{L}\Delta v_{g}(t) \\ &= -\frac{R}{L}\Delta i_g(t) - \frac{1}{L}(\Delta n_u(t) v_{cu0}^{\Sigma} + n_{u0}(t)\Delta v_{cu}^{\Sigma} + \Delta n_l(t) v_{cl0}^{\Sigma} + n_{l0}(t)\Delta v_{cl}^{\Sigma}) \\ &\quad - \frac{2}{L}\Delta v_{g}(t) \end{aligned} \tag{49}$$

$$\frac{d\Delta v_{cu}^{\Sigma}(t)}{dt} = \frac{n_{u0}(t)\Delta i_u(t) + \Delta n_u(t) i_{u0}}{C_{arm}} \tag{50}$$

$$\frac{d\Delta v_{cl}^{\Sigma}(t)}{dt} = \frac{n_{l0}(t)\Delta i_l(t) + \Delta n_l(t) i_{l0}}{C_{arm}} \tag{51}$$

In those equations, the subscripts '0' and 'Δ' denote steady-state and perturbation components, respectively. The injected small perturbation voltage leads to perturbations in all variables at frequencies of $\Delta\omega, \Delta\omega \pm \omega_1, \Delta\omega \pm 2\omega_1, \ldots, \Delta\omega \pm h\omega_1$. Those frequencies may have significant effects on the MMC impedance response, and thus all those frequency components are included in the impedance modelling.

Rewriting (48)-(51) in the matrix form, the small-signal state-space equation is obtained:

$$\Delta\dot{x}(t) = A_p(t)\Delta x(t) + B_p(t)\Delta u(t) \tag{52}$$

where

$$\Delta x(t) = \left[\Delta i_c(t), \Delta v_{cu}^{\Sigma}(t), \Delta v_{cl}^{\Sigma}(t), \Delta i_g(t)\right]^T \tag{53}$$

$$\Delta u(t) = \left[\Delta n_u(t), \Delta n_l(t), \Delta v_g(t)\right]^T \tag{54}$$

$$A_p(t) = \begin{bmatrix} -\frac{R}{L} & -\frac{n_{u0}(t)}{2L} & -\frac{n_{l0}(t)}{2L} & 0 \\ \frac{n_{u0}(t)}{C_{arm}} & 0 & 0 & \frac{n_{u0}(t)}{2C_{arm}} \\ \frac{n_{l0}(t)}{C_{arm}} & 0 & 0 & -\frac{n_{l0}(t)}{2C_{arm}} \\ 0 & -\frac{n_{u0}(t)}{L} & -\frac{n_{l0}(t)}{L} & -\frac{R+2Z_L}{L} \end{bmatrix} \tag{55}$$

$$B_p(t) = \begin{bmatrix} -\frac{v_{cu0}^{\Sigma}(t)}{2L} & -\frac{v_{cl0}^{\Sigma}(t)}{2L} & 0 \\ \frac{i_{c0}(t)+\frac{i_{g0}(t)}{2}}{C_{arm}} & 0 & 0 \\ 0 & \frac{i_{c0}(t)-\frac{i_{g0}(t)}{2}}{C_{arm}} & 0 \\ -\frac{v_{cu0}^{\Sigma}(t)}{L} & \frac{v_{cl0}^{\Sigma}(t)}{L} & -\frac{2}{L} \end{bmatrix} \tag{56}$$

Applying the HSS modelling procedure to (52)-(56), the time-domain state-space equations of the MMC is transformed in the small-signal HSS model, as expressed as:

$$s\Delta\mathbb{X} = \left(\mathbb{A}_p - \mathbb{Q}_p\right)\Delta\mathbb{X} + \mathbb{B}_p\Delta\mathbb{U} \tag{57}$$

The variables of $\Delta\mathbb{X}$, $\Delta\mathbb{U}$ and $\mathbb{Q}_p$ in (57) are given in (58)-(60), where the subscript 'p', '$p+1$',…, '$p+h$' denotes the perturbation component at frequency $\Delta\omega, \Delta\omega \pm \omega_1, \ldots, \Delta\omega \pm h\omega_1$, respectively. The Toeplitz matrices $\mathbb{A}_p$ and $\mathbb{B}_p$ related to the control system of the MMC can be expressed as (41)-(46) when open-loop control is applied. The HSS model of the MMC with closed-loop control is given in the Chapter 4.

$$\Delta\mathbb{X} = \left[X_{p-h}, \dots, X_{p-1}, X_p, X_{p+1}, \dots, X_{p+h}\right]^T$$
$$X_{p\pm h} = \left[I_{cp\pm h}, V^{\Sigma}_{cup\pm h}, V^{\Sigma}_{clp\pm h}, I_{gp\pm h}\right] \tag{58}$$

$$\Delta\mathbb{U} = \left[U_{p-h}, \dots, U_{p-1}, U_p, U_{p+1}, \dots, U_{p+h}\right]^T$$
$$U_p = \left[V_p\right] \tag{59}$$
$$U_{p\pm h} = [0], (h \geq 1)$$

$$\mathbb{Q}_p = diag\left[j\left(\omega_p - h\omega_1\right)\cdot I, \dots, j\left(\omega_p - \omega_1\right)\cdot I, j\omega_p \cdot I, j\left(\omega_p + \omega_1\right)\cdot I, \dots, j\left(\omega_p + h\omega_1\right)\cdot I\right] \tag{60}$$

3.3 Impedance model validation

3.3.1 HSS-based impedance model of the MMC

The small-signal impedance model of the MMC is derived in this section. The small-signal HSS model developed in Section 3.2.2 shows the relationship between state variables $\Delta\mathbb{X}$ and input variables $\Delta\mathbb{U}$. The AC-side current perturbation ΔI_g in state variables $\Delta\mathbb{X}$ is the response of the MMC system to the small sinusoidal perturbation AC-side voltage ΔV_g at frequency ω_p. The AC-side small-signal impedance of the MMC is obtained by calculating the ratio of the perturbation voltage ΔV_g to the response current ΔI_g at frequency ω_p, as:

$$Z_{MMC}\left(j\omega_p\right) = \frac{\Delta V_g}{\Delta I_g} \tag{61}$$

where ΔV_g and ΔI_g are the complex phasors of the resulting perturbation voltage and current at the frequency ω_p.

3.3.2 Impedance model validation

In order to validate the HSS model developed in this work, a comparison between the impedance plots from the HSS model and the time-domain model has been carried out. The time-domain models are implemented in RTDS, PSCAD and MATLAB/Simulink, and the HSS model as described in this section is implemented by using an m.file in MATLAB. The different simulation platforms are used as shown in Figure 5 to take advantages of the automated process in Simulink in the initial development stage so issues can be discovered quickly. Open-loop model as shown in Figure 4 is applied first by directly setting the fundamental frequency and second harmonic components as expressed in (36) and (37) as the references. The main electrical parameters of the MMC system are listed in Table 1.

In time-domain simulations, the AC-side small-signal impedance of the MMC is measured by means of injecting a series of small perturbation voltage signals ΔV_p of which the peak value equals to 1kV at different frequencies in the AC-side of the MMC as shown in Figure 4. The AC-side current response ΔI_g of the MMC system is measured together with the terminal voltage ΔV_g at corresponding frequency, and the impedance under this frequency is calculated by applying (61). In PSCAD and MATLAB/Simulink the simulation is carried out with 5μs time-step. In RTDS simulation, the large simulation time-step is 25 μs and the small time-step is 2.5 μs.

Table 1 Main electrical parameters of the MMC system

Parameters	Value
MMC rated apparent power (Sn)	1265 MVA
MMC rated active power (P)	±1200 MW
MMC rated reactive power(Q)	±400 MVAr
MMC nominal DC Voltage (V_{dc})	640 kV(±320 kV)
MMC rated AC output voltage (L-L)	360 kV
Arm inductance (L_{arm})	0.13 pu
Cell capacitance (C_{SM})	31.4 μF
Nominal Frequency	50 Hz
Transformer rated apparent power	1265 MVA
Interfacing transformer voltage ratio	400/360 kV
Transformer leakage reactance	0.18 pu
Transformer resistance	0.004452 pu

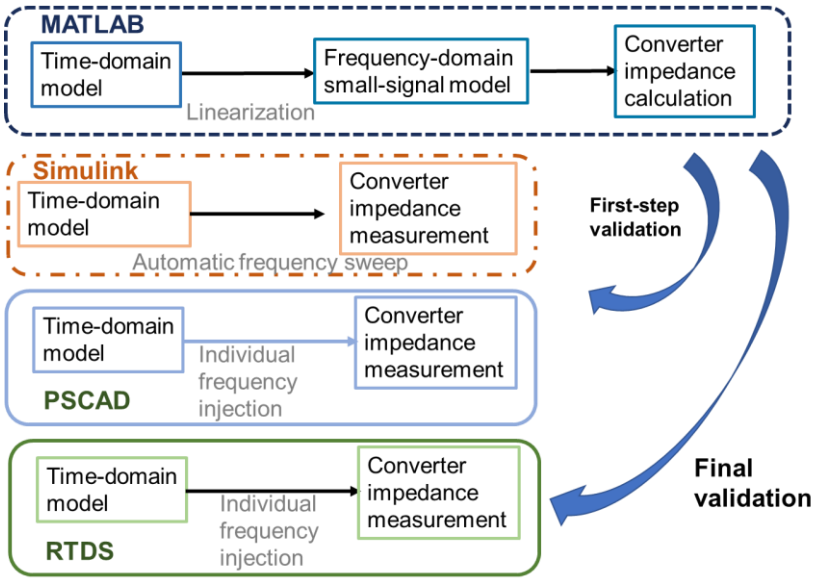

Figure 5: The validation process of the analytical model

The impedance plots of the HSS model are shown in Figure 6 with considered harmonic orders $h = 0,1,2,3,4$, comparing with that of the Simulink time-domain model shown in the same figure. It can be observed that the harmonic order considered in the HSS model of the MMC has a great impact on the accuracy of the analytical impedance model. Since significant steady-state harmonic components exist in the arm current and capacitor voltage of the MMC, the higher the harmonic order considered in the HSS model, the more accurate the analytical impedance model. In the impedance magnitudes shown in Figure 6, the solid red line which represents the magnitude of the HSS impedance model with h=4 overlap with that of the Simulink time-domain model which is shown as blue star markers in the figure. In the impedance phases shown in Figure 6, the close overlap between those two models can also be observed. Based on those observations, it can be indicated that the analytical model with h=4 matches well with the measured result in the Simulink time-domain simulation.

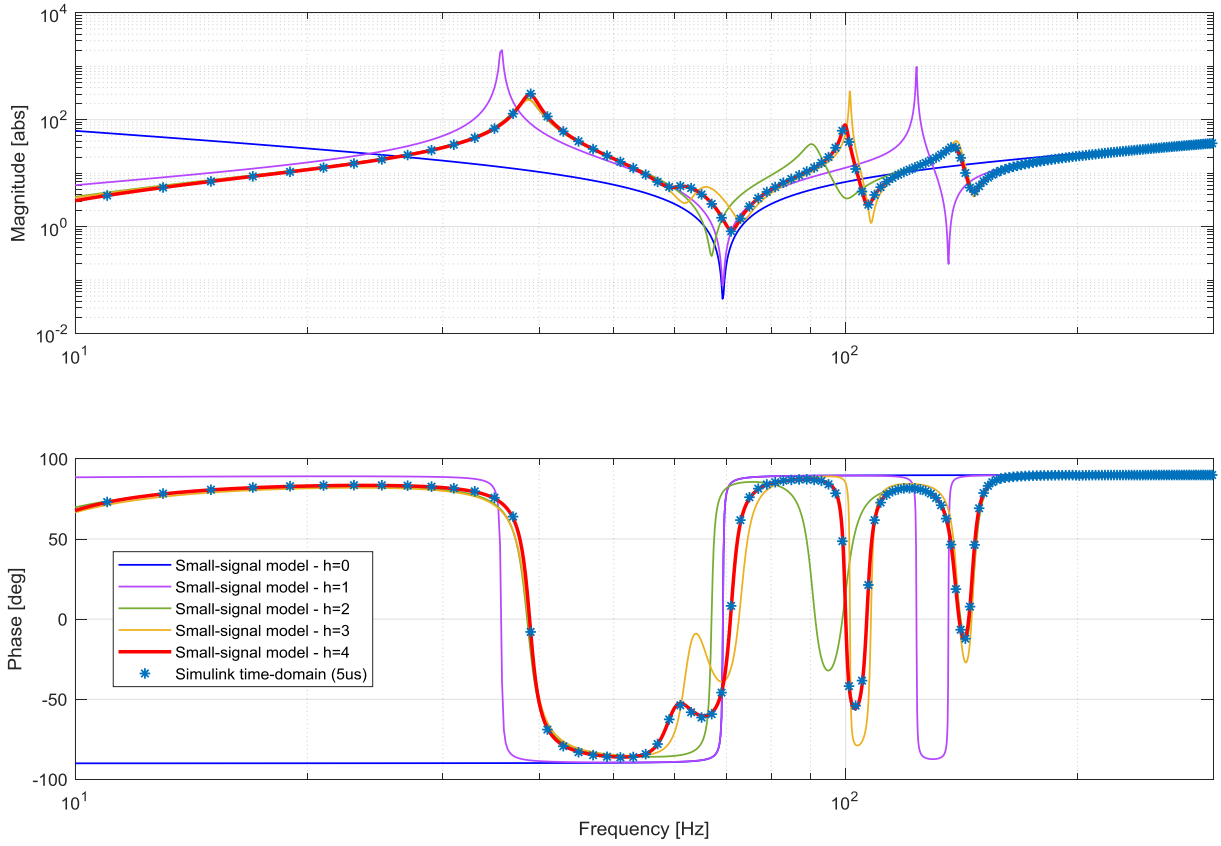

Figure 6: The impedance plot of HSS model and Simulink time-domain model

Figure 7 shows the AC-side small-signal impedance comparison among the four different time-domain models and the analytical HSS model with h=4. The Simulink model and the PSCAD model with 5μs simulation time-step match well to that of the analytical model in both magnitude and phase. While the RTDS model with 25μs large time-step (for control part) and 2.5μs small time-step (for power circuit) shows some differences at 40Hz and 50-80Hz especially for the phases compared with the results from the Simulink and PSCAD models with 5μs simulation time-step. To investigate further, PSCAD model with

25μs simulation time-step has been added in this comparison. The violet markers which represent the PSCAD model with 25μs show similar trends at corresponding frequencies with the RTDS model. This indicates that the simulation time-step influence the accuracy of time-domain measured impedance and in particular the phases. This implies that caution must be taken if impedances measured from RTDS models with large time step are used, especially if phase margin is of concern.

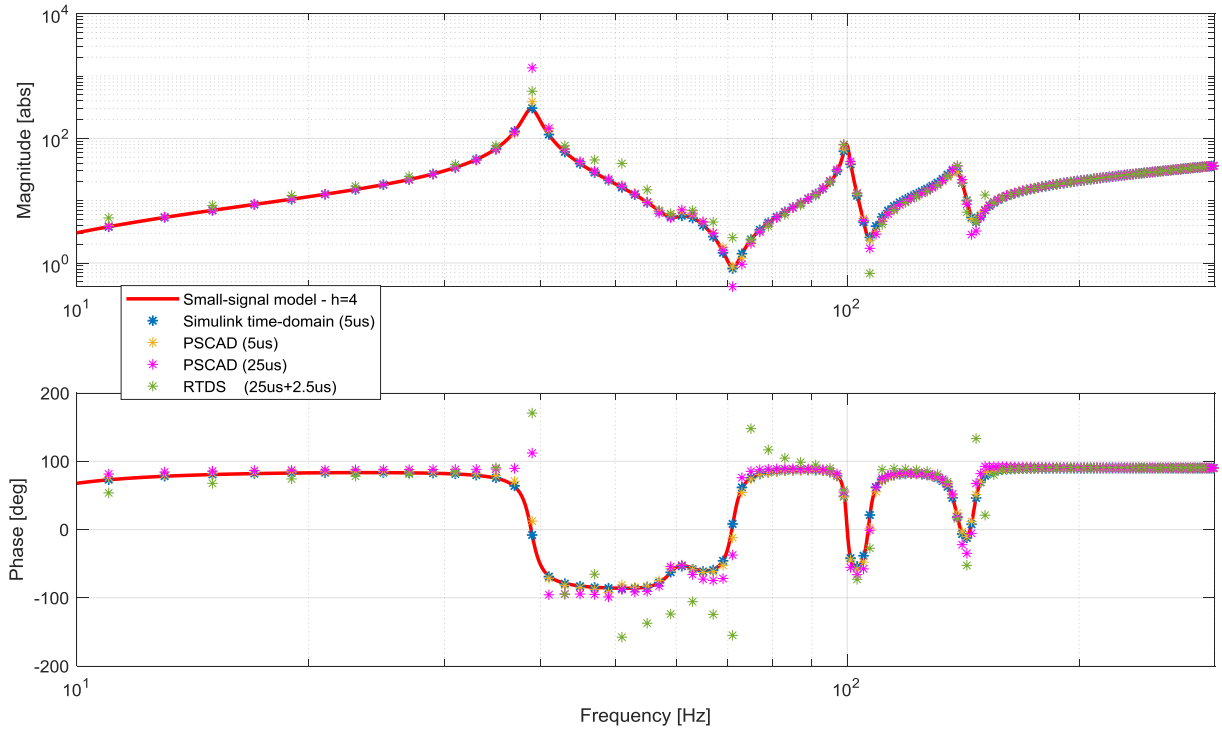

Figure 7 Impedance plot of the HSS model (h=4) and time-domain models

4 Small-signal MMC impedance with full control system

4.1 Principle of MMC control

4.1.1 Inner fundamental current controller

Considering AC current in the dq reference frame, the dynamic i_d and i_q can be expressed as [5]:

$$\begin{aligned}\frac{di_d}{dt} &= -\frac{R_e}{L_e} i_d + \frac{v_{cd}^* - v_d + \omega L_e i_q}{L_e} \\ \frac{di_q}{dt} &= -\frac{R_e}{L_e} i_q + \frac{v_{cq}^* - v_q - \omega L_e i_d}{L_e}\end{aligned} \tag{62}$$

where, v_{cd}^* and v_{cq}^* are the equivalent AC voltage generated by the MMC at d- and q-axis, R_e and L_e are the equivalent input AC resistance and inductance respectively (equal to half of the resistance and inductance of the arm reactor), v_d and v_q are the network voltages at the MMC AC terminal. As R_e is usually very small, it is thus neglected in the following analysis.

Notice that the two unknowns in (62) are v_{cd}^* and v_{cq}^*. To facilitate estimations of v_{cd}^* and v_{cq}^* using proportional-integral (PI) controllers, the terms $v_{cd}^* - v_d + \omega L_e i_q$ and $v_{cq}^* - v_d - \omega L_e i_d$ are replaced by u_d and u_q, which represent the outputs of the PI controllers in the d and q axis (i.e., $u_d = v_{cd}^* - v_d + \omega L_e i_q$ and $u_q = v_{cq}^* - v_d - \omega L_e i_d$. Since u_d and u_q represent the outputs of the current controllers that regulate i_d and i_q, they are expressed as:

$$\begin{aligned}u_d(t) &= K_P^i (i_d^* - i_d) + K_I^i \int (i_d^* - i_d) dt \\ u_q(t) &= K_P^i (i_q^* - i_q) + K_I^i \int (i_q^* - i_q) dt\end{aligned} \tag{63}$$

As the PI controllers on the d and q channels facilitate computations of u_d and u_q as shown in (63), the v_{cd}^* and v_{cq}^* can be calculated from the PI outputs (u_d and u_q) as:

$$\begin{aligned}v_{cd}^* &= u_d + v_d - \omega L_e i_q \\ v_{cq}^* &= u_q + v_d + \omega L_e i_d\end{aligned} \tag{64}$$

On the basis of (63) and (64), the block diagram in Figure 8 is drawn. v_{cd}^{*}, v_{cq}^{*}, $\omega L_e i_q$ and $\omega L_e i_d$ in (64) represent the feedforward terms of the current controller.

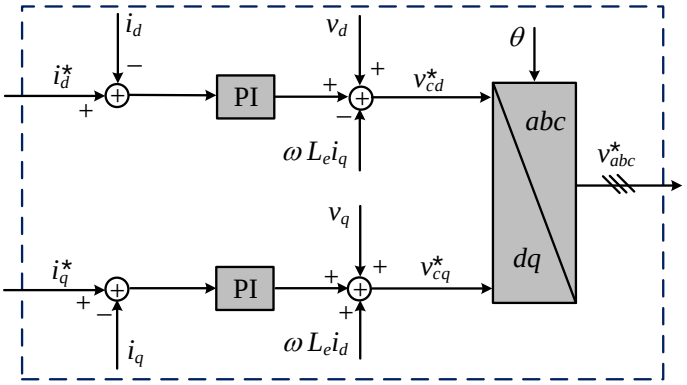

Figure 8: A generic block diagram of an Inner Current Controller

After the merger of (62), (63) and (64), and further algebraic manipulations, where the integral parts of u_d and u_q are replaced by λ_d and λ_q, the following state space equation is obtained:

$$\frac{d}{dt}\begin{bmatrix} i_d \\ \lambda_d \\ i_q \\ \lambda_q \end{bmatrix} = \begin{bmatrix} -\dfrac{R_e + K_P^i}{L_e} & \dfrac{1}{L_e} & 0 & 0 \\ -K_I^i & 0 & 0 & 0 \\ 0 & 0 & -\dfrac{R_e + K_P^i}{L_e} & \dfrac{1}{L_e} \\ 0 & 0 & -K_I^i & 0 \end{bmatrix} \begin{bmatrix} i_d \\ \lambda_d \\ i_q \\ \lambda_q \end{bmatrix} + \begin{bmatrix} \dfrac{K_P^i}{L_e} & 0 \\ K_I^i & 0 \\ 0 & \dfrac{K_P^i}{L_e} \\ 0 & K_I^i \end{bmatrix} \begin{bmatrix} i_d^* \\ i_q^* \end{bmatrix} \tag{65}$$

After transforming (65) into s-domain using Laplace transform and matrix manipulation, the closed transfer function of the current controller for both channels is:

$$\frac{i_d(s)}{i_d^*(s)} = \frac{i_q(s)}{i_q^*(s)} = \frac{K_P^i / L_e \, s + K_I^i / L_e}{s^2 + (K_P^i + R_e)/L_e \, s + K_I^i / L_e} \tag{66}$$

After comparing the denominator of (66) with that of the standard transfer function of a 2nd order system, the proportional and integral constants or gains of the current controllers are expressed as: $K_P^i = 2\omega_n \zeta L_e$ and $K_I^i = \omega_n^2 L_e$, where, the natural frequency ω_n and damping factor ζ can be selected, considering a number of control objectives such as settling time or peak overshoot. However, the final gains must be fine-tuned to ensure satisfactory performance over the entire system operating range.

4.1.2 Circulating Current Controller (CCC)

Subtracting (23) from (22), the following equation is obtained for one phase:

$$\tfrac{1}{2}V_{dc} - \tfrac{1}{2}(v_u + v_l) = R\tfrac{1}{2}(i_u + i_l) + L\frac{d}{dt}\tfrac{1}{2}(i_u + i_l) \tag{67}$$

Defining the common-mode current as $i_c = \tfrac{1}{2}(i_u + i_v)$ and the common-mode component of the phase voltage as $v_u + v_l = \alpha_d V_{carm}$, (67) can be reduced to:

$$\tfrac{1}{2}\left(V_{dc} - \alpha_d V_{carm}\right) = Ri_c + L\frac{di_c}{dt} \tag{68}$$

It is worth emphasizing that the common-mode capacitor sum, $v_u + v_l = \alpha_d V_{carm} + \Delta v_{carm}$ used to describe the synthesis of the arm voltages, consists of DC component 'V_{carm}' that determines the dc component of the common-mode current and ac component 'Δv_{carm}' which is seen as voltage ripple that drives the circulating current in phase leg. Taking these assertions into account, equation (68) can be rewritten as:

$$\tfrac{1}{2}\left[V_{dc} - \left(\alpha_d V_{carm} + \Delta v_{carm}\right)\right] = Ri_c + L\frac{di_c}{dt} \tag{69}$$

Using the following definition of the common-mode currents, $i_c = I_d + i_h$, (69) can be separated into AC and DC components as:

$$\tfrac{1}{2}\left[V_{dc} - \alpha_d V_{carm}\right] = RI_d + L\frac{dI_d}{dt} \tag{70}$$

$$-\tfrac{1}{2}\Delta v_{carm} = Ri_h + L\frac{di_h}{dt} \tag{71}$$

where I_d represents the DC component of the upper and lower arm currents, and i_h is the inherent harmonic current in the upper and lower arm currents.

Equation (71) can be used in design of the circulating current controller. After renaming or replacing the term $-\tfrac{1}{2}\Delta v_{carm}$ by Δv_{cir}, a PI based circulating current controller (CCC) can be defined as in terms of three-phase quantities:

$$\begin{aligned}
\Delta v_{cir}^{a} &= K_P^{cir}(i_h^{a*} - i_h^{a}) + K_I^{cir}\int (i_h^{a*} - i_h^{a})dt \\
\Delta v_{cir}^{b} &= K_P^{cir}(i_h^{b*} - i_h^{b}) + K_I^{cir}\int (i_h^{b*} - i_h^{b})dt \\
\Delta v_{cir}^{c} &= K_P^{cir}(i_h^{c*} - i_h^{c}) + K_I^{cir}\int (i_h^{c*} - i_h^{c})dt
\end{aligned} \tag{72}$$

Since this controller acts on the common-mode component of the modulation functions of the upper and lower arms in each phase leg, its output must be added with the same sign to modulation functions of the upper and lower arms. But because of the difficulty of tuning of PI controller when it is used to regulate sinusoidal quantities, the actual circulating current suppression controller is implemented using proportional-resonant (PR) control. The time-domain implementation of an ideal PR controller is depicted in Figure 9. From Figure 9, the basic equations that describe PR controller are:

$$\begin{aligned}
\Delta v_{cir}^{a} &= K_P^{cir}(i_h^{a*} - i_h^{a}) + \int\left[K_I^{cir}(i_h^{a*} - i_h^{a}) - x_a\right]dt \\
x_a &= \omega_n^2 \int y_a dt \\
\Delta v_{cir}^{b} &= K_P^{cir}(i_h^{b*} - i_h^{b}) + \int\left[K_I^{cir}(i_h^{b*} - i_h^{b}) - x_b\right]dt \\
x_b &= \omega_n^2 \int y_b dt \\
\Delta v_{cir}^{c} &= K_P^{cir}(i_h^{c*} - i_h^{c}) + \int\left[K_I^{cir}(i_h^{c*} - i_h^{c}) - x_c\right]dt \\
x_c &= \omega_n^2 \int y_c dt
\end{aligned} \tag{73}$$

Since the objective is to suppress the circulating currents which are dominantly 2nd order harmonic, the references for the circulating currents must be set to zero and ω_n must be set at twice of the fundamental frequency. The overall circulating current controller is shown in Figure 10.

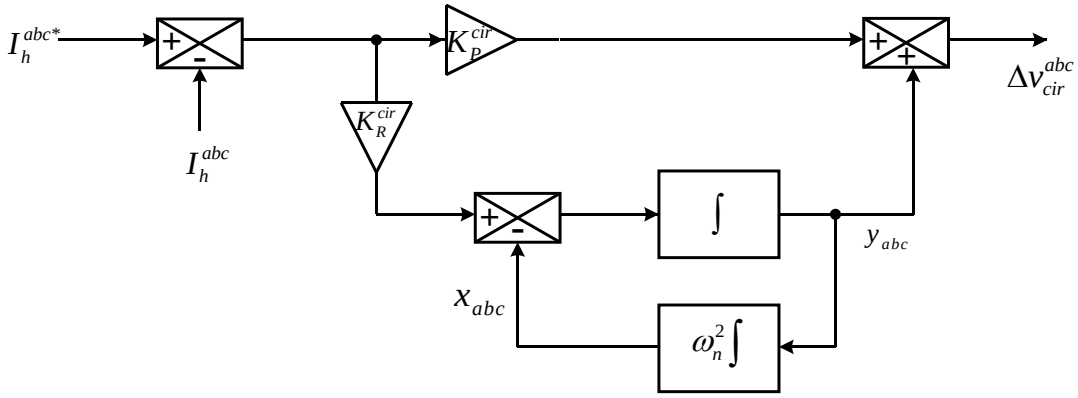

Figure 9: Graphical depiction of PR controller

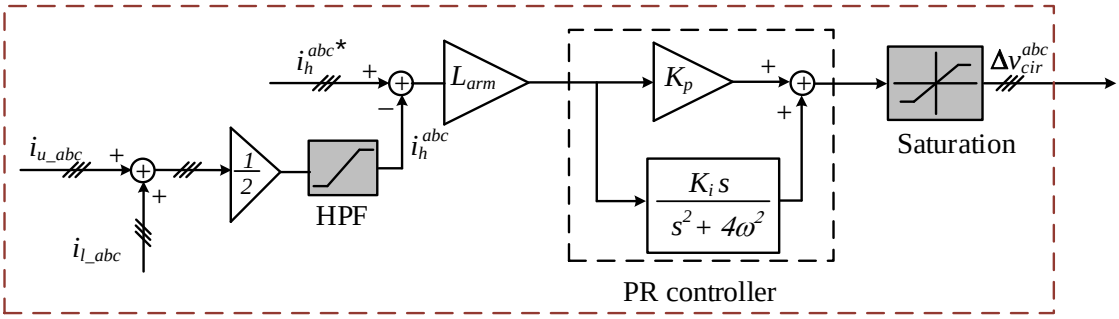

Figure 10: Complete implementation of the circulating current control in s-domain

4.2 Small-signal modelling of MMC control system

In order to consider the effects of the controller on the small-signal MMC impedance and applying the HSS method, it is necessary to calculate the small-signal transfer function from the measured plant signals to the MMC modulation index (control output).

4.2.1 Small-signal model of current controller

The outputs $m_{d,c}$ and $m_{q,c}$ of the dq current controller are calculated as:

$$m_d(s) = \frac{1}{V_{DC}}[G_{PI}(s)(i_d^* - i_d) + G_{VFF}(s)V_d - \omega_0 L_f i_q] \tag{74}$$

$$m_q(s) = \frac{1}{V_{DC}}[G_{PI}(s)(i_q^* - i_q) + G_{VFF}(s)V_q + \omega_0 L_f i_d] \tag{75}$$

Linearizing (74) and (75) yields the corresponding small-signal expressions $\Delta m_d(s)$ and $\Delta m_q(s)$:

$$\Delta m_d(s) = \frac{1}{V_{DC}}[-G_{PI}(s)\Delta i_d + G_{VFF}(s)\Delta V_d - \omega_0 L_f \Delta i_q] \tag{76}$$

$$\Delta m_q(s) = \frac{1}{V_{DC}}[-G_{PI}(s)\Delta i_q + G_{VFF}(s)\Delta V_q + \omega_0 L_f \Delta i_d] \tag{77}$$

Equations (76)-(77) enable the calculation of the open-loop transfer functions from $\Delta V_{dq}$to $\Delta m_{dq,V}$ and from Δi_{dq} to $\Delta m_{dq,c}$:

$$\Delta m_{dq,V} = \frac{1}{V_{DC}}\begin{bmatrix} G_{VFF}(s) & 0 \\ 0 & G_{VFF}(s) \end{bmatrix}\Delta V_{dq} \tag{78}$$

$$\Delta m_{dq,c} = -\frac{1}{V_{DC}}\begin{bmatrix} G_{PI}(s) & 0 \\ 0 & G_{PI}(s) \end{bmatrix}\Delta i_{dq} + \frac{1}{V_{DC}}\begin{bmatrix} 0 & -\omega_0 L_f \\ \omega_0 L_f & 0 \end{bmatrix}\Delta i_{dq} \tag{79}$$

The impedance analysis of the system is carried out in *abc* reference frame and thus the dynamics equations (78)-(79) in *dq* reference frame need to be transformed into *abc*-frame. The used transformation matrices are derived as follows.

The transfer function matrix defined in the *dq-frame* reference frame is governed by:

$$y_{dq}(s) = \begin{bmatrix} G(s) & 0 \\ 0 & G(s) \end{bmatrix} x_{dq}(s) \tag{80a}$$

and the corresponding equation in the *abc*-frame is:

$$y_{abc}(s) = \begin{bmatrix} \frac{1}{3}[G(s-j\omega_0)+G(s+j\omega_0)] & \frac{1}{3}[G(s-j\omega_0)e^{j\frac{2}{3}\pi}+G(s+j\omega_0)e^{-j\frac{2}{3}\pi}] & \frac{1}{3}[G(s-j\omega_0)e^{j\frac{4}{3}\pi}+G(s+j\omega_0)e^{-j\frac{4}{3}\pi}] \\ \frac{1}{3}[G(s-j\omega_0)e^{-j\frac{2}{3}\pi}+G(s+j\omega_0)e^{j\frac{2}{3}\pi}] & \frac{1}{3}[G(s-j\omega_0)+G(s+j\omega_0)] & \frac{1}{3}[G(s-j\omega_0)e^{j\frac{2}{3}\pi}+G(s+j\omega_0)e^{-j\frac{2}{3}\pi}] \\ \frac{1}{3}[G(s-j\omega_0)e^{-j\frac{4}{3}\pi}+G(s+j\omega_0)e^{j\frac{4}{3}\pi}] & \frac{1}{3}[G(s-j\omega_0)e^{-j\frac{2}{3}\pi}+G(s+j\omega_0)e^{j\frac{2}{3}\pi}] & \frac{1}{3}[G(s-j\omega_0)+G(s+j\omega_0)] \end{bmatrix} x_{abc}(s) \tag{80b}$$

Particularly, the cross-coupling terms of the current controller need to be considered and transformed from *dq* reference frame to *abc* frame. Considering the following relation

$$y_{dq}(s) = \begin{bmatrix} 0 & -\omega_0 L_f \\ \omega_0 L_f & 0 \end{bmatrix} x_{dq}(s) \tag{81a}$$

the cross-coupling terms be reformulated in the *abc* frame as:

$$y_{abc}(s) = \begin{bmatrix} 0 & \frac{2}{3}\omega_0 L_f \sin(\frac{2}{3}\pi) & \frac{2}{3}\omega_0 L_f \sin(\frac{4}{3}\pi) \\ -\frac{2}{3}\omega_0 L_f \sin(\frac{2}{3}\pi) & 0 & \frac{2}{3}\omega_0 L_f \sin(\frac{2}{3}\pi) \\ -\frac{2}{3}\omega_0 L_f \sin(\frac{4}{3}\pi) & -\frac{2}{3}\omega_0 L_f \sin(\frac{2}{3}\pi) & 0 \end{bmatrix} x_{abc}(s) \tag{81b}$$

In (80) and (81), it has been assumed that $x_{abc}(t)$ is a generic 3 phase balanced signal at frequency ω_0. Defining

$$\Delta m_{dq} = \Delta m_{dq,V} + \Delta m_{dq,c} \tag{80}$$

and the matrices in (78) and (79) can be mapped to the *abc* frame by applying (80) and (81) as:

$$\Delta m_{abc} = \Delta m_{abc,V} + \Delta m_{abc,c}$$

where

$$\Delta m_{abc,c} = \frac{1}{V_{DC}} G_{c,abc}(s) \Delta i_{abc}(s) \tag{81}$$

$$\Delta m_{abc,V} = \frac{1}{V_{DC}} G_{V,abc}(s)\Delta V_{abc}(s) \tag{82}$$

In (81), the transfer function is depicted as:

$$G_{c,abc}(s) = -G_{PI,abc}(s) + G_{I,abc}(s)$$

where

$$G_{PI,abc}(s) = \begin{bmatrix} \frac{1}{3}[G_{PI}(s-j\omega_0)+G_{PI}(s+j\omega_0)] & \frac{1}{3}[G_{PI}(s-j\omega_0)e^{j\frac{2}{3}\pi}+G_{PI}(s+j\omega_0)e^{-j\frac{2}{3}\pi}] & \frac{1}{3}[G_{PI}(s-j\omega_0)e^{j\frac{4}{3}\pi}+G_{PI}(s+j\omega_0)e^{-j\frac{4}{3}\pi}] \\ \frac{1}{3}[G_{PI}(s-j\omega_0)e^{-j\frac{2}{3}\pi}+G_{PI}(s+j\omega_0)e^{j\frac{2}{3}\pi}] & \frac{1}{3}[G_{PI}(s-j\omega_0)+G_{PI}(s+j\omega_0)] & \frac{1}{3}[G_{PI}(s-j\omega_0)e^{j\frac{2}{3}\pi}+G_{PI}(s+j\omega_0)e^{-j\frac{2}{3}\pi}] \\ \frac{1}{3}[G_{PI}(s-j\omega_0)e^{-j\frac{4}{3}\pi}+G_{PI}(s+j\omega_0)e^{j\frac{4}{3}\pi}] & \frac{1}{3}[G_{PI}(s-j\omega_0)e^{-j\frac{2}{3}\pi}+G_{PI}(s+j\omega_0)e^{j\frac{2}{3}\pi}] & \frac{1}{3}[G_{PI}(s-j\omega_0)+G_{PI}(s+j\omega_0)] \end{bmatrix}$$

$$G_{I,abc}(s) = \begin{bmatrix} 0 & \frac{2}{3}\omega_0 L_f \sin(\frac{2}{3}\pi) & \frac{2}{3}\omega_0 L_f \sin(\frac{4}{3}\pi) \\ -\frac{2}{3}\omega_0 L_f \sin(\frac{2}{3}\pi) & 0 & \frac{2}{3}\omega_0 L_f \sin(\frac{2}{3}\pi) \\ -\frac{2}{3}\omega_0 L_f \sin(\frac{4}{3}\pi) & -\frac{2}{3}\omega_0 L_f \sin(\frac{2}{3}\pi) & 0 \end{bmatrix}$$

$$G_{V,abc}(s) = \begin{bmatrix} \frac{1}{3}[G_{VFF}(s-j\omega_0)+G_{VFF}(s+j\omega_0)] & \frac{1}{3}[G_{VFF}(s-j\omega_0)e^{j\frac{2}{3}\pi}+G_{VFF}(s+j\omega_0)e^{-j\frac{2}{3}\pi}] & \frac{1}{3}[G_{VFF}(s-j\omega_0)e^{j\frac{4}{3}\pi}+G_{VFF}(s+j\omega_0)e^{-j\frac{4}{3}\pi}] \\ \frac{1}{3}[G_{VFF}(s-j\omega_0)e^{-j\frac{2}{3}\pi}+G_{VFF}(s+j\omega_0)e^{j\frac{2}{3}\pi}] & \frac{1}{3}[G_{VFF}(s-j\omega_0)+G_{VFF}(s+j\omega_0)] & \frac{1}{3}[G_{VFF}(s-j\omega_0)e^{j\frac{2}{3}\pi}+G_{VFF}(s+j\omega_0)e^{-j\frac{2}{3}\pi}] \\ \frac{1}{3}[G_{VFF}(s-j\omega_0)e^{-j\frac{4}{3}\pi}+G_{VFF}(s+j\omega_0)e^{j\frac{4}{3}\pi}] & \frac{1}{3}[G_{VFF}(s-j\omega_0)e^{-j\frac{2}{3}\pi}+G_{VFF}(s+j\omega_0)e^{j\frac{2}{3}\pi}] & \frac{1}{3}[G_{VFF}(s-j\omega_0)+G_{VFF}(s+j\omega_0)] \end{bmatrix}$$

The small-signal outputs of the current controller in *abc-frame* reference frame is summarised as:

$$\Delta m_{abc} = \frac{1}{V_{DC}}[G_{c,abc}(s)\Delta i_{abc} + G_{V,abc}(s)\Delta V_{abc}] \tag{83}$$

4.2.2 The small-signal model of circulating current controller

The controller modulation index m_{cc} associated to the circulating current controller is calculated as:

$$m_{cc} = \frac{1}{V_{DC}}[(i_c^* - \frac{G_h s^2}{s^2+2\xi_h\omega_h s+\omega_h^2} i_c)G_{PR}(s)] \tag{84}$$

Linearizing (84) at steady operating point yields the corresponding small-signal equivalent expression:

$$\Delta m_{cc} = -\frac{1}{V_{DC}} \frac{G_h s^2}{s^2+2\xi_h\omega_h s+\omega_h^2} G_{PR}(s)\Delta i_c = \frac{1}{V_{DC}} G_{cc}(s)\Delta i_c \tag{85}$$

For the *h*-th harmonic perturbation component in the model, the relationship between Δm_{cc} and Δi_c can be expressed as:

$$\Delta m_{cc}(s+jh\omega_0) = \frac{1}{V_{DC}} G_{cc}(s+jh\omega_0)\Delta i_c(s+jh\omega_0) \tag{86}$$

where $G_{cc}(s+jh\omega_0)$ denotes the transfer function $G_{cc}(s)$ making $h\omega_0$ frequency shift. Considered frequency shift, Toeplitz matric $\mathbb{A}$ is rewritten as:

$$\mathbb{A}' = \begin{bmatrix} A_0(s-jh\omega_0) & A_{-1}(s-j(h-1)\omega_0) & \dots & A_{-h}(s+j\omega_0) & & & \\ A_1(s-jh\omega_0) & \ddots & \ddots & \ddots & \ddots & & \\ \vdots & \ddots & A_0 & A_{-1}(s+j\omega_0) & \ddots & \ddots & \\ A_h(s-jh\omega_0) & \ddots & A_1 & A_0(s+j\omega_0) & A_{-1}(s+j2\omega_0) & \ddots & A_{-h}(s+jh\omega_0) \\ & \ddots & \ddots & A_1(s+j\omega_0) & A_0(s+j2\omega_0) & \ddots & \vdots \\ & & \ddots & \ddots & \ddots & \ddots & A_{-1}(s+jh\omega_0) \\ & & & A_h(s+j\omega_0) & \dots & A_1(s+j(h-1)\omega_0) & A_0(s+jh\omega_0) \end{bmatrix} \tag{87}$$

where $A_0(s+j\omega_0)$, $A_0(s+j2\omega_0)$,…, $A_0(s+jh\omega_0)$ represent all the transfer functions in A_0 matric making $j\omega_0$, $j2\omega_0$, …, $jh\omega_0$ frequency shift respectively.

As the circulating current controller is implemented in the *abc*-frame frame, its small-signal matrix formulation is:

$$\Delta m_{cc,abc} = \frac{1}{V_{DC}} \begin{bmatrix} G_{cc}(s) & 0 & 0 \\ 0 & G_{cc}(s) & 0 \\ 0 & 0 & G_{cc}(s) \end{bmatrix} \Delta i_{c,abc} \tag{88}$$

4.3 Impedance of MMC with control system

4.3.1 Complete system modelling

The control system of the MMC only influences the switching function of the upper and lower arms and thus the dynamic equations of the MMC circuit depicted by (22)-(33) in Section 3.2.1 is still valid for the MMC system when the full controllers are added. With the controllers added, the updated switching function for upper and lower arms are defined in (89) and (90), respectively:

$$n_{u(t)} = \frac{1}{V_{dc}} \left(\frac{1}{2} V_{dc} - G_v Z_L i_g(t) - G_c i_g(t) - G_{cc} i_c(t) \right) \tag{89}$$

$$n_{l(t)} = \frac{1}{V_{dc}} \left(\frac{1}{2} V_{dc} + G_v Z_L i_g(t) + G_c i_g(t) - G_{cc} i_c(t) \right) \tag{90}$$

Based on (22)-(33) in Section 3.2.1, and (89) and (90), the small-signal of the MMC with full controllers can be expressed as

$$\Delta n_u(t) = \frac{1}{V_{dc}} \left[-(G_v Z_L + G_c) \Delta i_g(t) - G_{cc} \Delta i_c(t) \right] \tag{91}$$

$$\Delta n_l(t) = \frac{1}{V_{dc}} \left[(G_v Z_L + G_c) \Delta i_g(t) - G_{cc\Delta} i_c(t) \right] \tag{92}$$

$$\begin{aligned}\Delta v_u(t) &= \Delta n_u(t) v_{cu0}^{\Sigma}(t) + n_{u0}(t)\Delta v_{cu}^{\Sigma}(t) \\ &= -(G_v Z_L + G_c) v_{cu0}^{\Sigma}(t)\Delta i_g(t) - G_{cc} v_{cu0}^{\Sigma}(t)\Delta i_c(t) + n_{u0}(t)\Delta v_{cu}^{\Sigma}(t)\end{aligned} \tag{93}$$

$$\begin{aligned}\Delta v_l(t) &= \Delta n_l(t) v_{cl0}^{\Sigma}(t) + n_l(t)\Delta v_{cl}^{\Sigma}(t) \\ &= (G_v Z_L + G_c) v_{cl0}^{\Sigma}(t)\Delta i_g(t) - G_{cc} v_{cl0}^{\Sigma}(t)\Delta i_c(t) + n_{l0}(t)\Delta v_{cl}^{\Sigma}(t)\end{aligned} \tag{94}$$

$$\begin{aligned}\frac{d\Delta v_{cu}^{\Sigma}(t)}{dt} &= \frac{i_{u0}(t)}{C_{arm}}\Delta n_u(t) + \frac{n_{u0}(t)}{C_{arm}}\Delta i_u(t) \\ &= \frac{n_{u0}(t) - G_{cc}(i_{c0}(t) + \frac{i_{g0}(t)}{2})}{C_{arm}}\Delta i_c(t) \\ &\quad + \frac{\frac{n_{u0}(t)}{2} - (G_v Z_L + G_c)(i_{c0}(t) + \frac{i_{g0}(t)}{2})}{C_{arm}}\Delta i_g(t)\end{aligned} \tag{95}$$

$$\begin{aligned}\frac{d\Delta v_{cl}^{\Sigma}(t)}{dt} &= \Delta n_l(t)\frac{i_{l0}(t)}{C_{arm}} + \frac{n_{l0}(t)}{C_{arm}}\Delta i_l(t) \\ &= \frac{-\frac{n_{l0}(t)}{2} + (G_v Z_L + G_c)\left(i_{c0}(t) - \frac{i_{g0}(t)}{2}\right)}{C_{arm}}\Delta i_g(t) \\ &\quad + \frac{n_{l0}(t) - G_{cc}\left(i_{c0}(t) - \frac{i_{g0}(t)}{2}\right)}{C_{arm}}\Delta i_c(t)\end{aligned} \tag{96}$$

$$\begin{aligned}\frac{d\Delta i_c(t)}{dt} &= -\frac{R}{L}\Delta i_c(t) - \frac{1}{2L}\Delta v_u(t) - \frac{1}{2L}\Delta v_l(t) \\ &= +\frac{(G_v Z_L + G_c)(v_{cu0}^{\Sigma}(t) - v_{cl0}^{\Sigma}(t))}{2L}\Delta i_g(t) \\ &\quad + \left(\frac{G_{cc}\left(v_{cu0}^{\Sigma}(t) + v_{cl0}^{\Sigma}(t)\right)}{2L} - \frac{R}{L}\right)\Delta i_c(t) - \frac{n_{u0}(t)}{2L}\Delta v_{cu}^{\Sigma}(t) \\ &\quad - \frac{n_{l0}(t)}{2L}\Delta v_{cl}^{\Sigma}(t)\end{aligned} \tag{97}$$

$$\begin{aligned}\frac{d\Delta i_g(t)}{dt} &= -\frac{2Z_L+R}{L}\Delta i_g(t) - \frac{1}{L}\Delta v_u(t) + \frac{1}{L}\Delta v_l(t) \\ &= \left(-\frac{2Z_L+R}{L} + \frac{(G_v Z_L + G_c)(v_{cu0}^{\Sigma}(t) + v_{cl0}^{\Sigma}(t))}{L}\right)\Delta i_g(t) \\ &+ \frac{G_{cc}\left(v_{cu0}^{\Sigma}(t) - v_{cl0}^{\Sigma}(t)\right)}{L}\Delta i_c(t) - \frac{n_{u0}(t)}{L}\Delta v_{cu}^{\Sigma}(t) + \frac{n_{l0}(t)}{L}\Delta v_{cl}^{\Sigma}(t)\end{aligned} \tag{98}$$

Rewriting (91)-(98) in the matrix form, the small-signal state-space can be obtained as

$$\Delta\dot{x}(t) = A_p(t)\Delta x(t) + B_p(t)\Delta u(t) \tag{99}$$

where

$$\Delta x(t) = \left[\Delta i_c(t), \Delta v_{cu}^{\Sigma}(t), \Delta v_{cl}^{\Sigma}(t), \Delta i_g(t)\right]^T \tag{100}$$

$$\Delta u(t) = \left[\Delta v_g(t)\right]^T \tag{101}$$

$$A_p(t) = \begin{bmatrix} \frac{G_{cc}\left(v_{cu0}^{\Sigma}(t)+v_{cl0}^{\Sigma}(t)\right)}{2L} - \frac{R}{L} & -\frac{n_{u0}(t)}{2L} & -\frac{n_{l0}(t)}{2L} & \frac{(G_v Z_L+G_c)(v_{cu0}^{\Sigma}(t)-v_{cl0}^{\Sigma}(t))}{2L} \\ \frac{n_{u0}(t)-G_{cc}\left(i_{c0}(t)+\frac{i_{g0}(t)}{2}\right)}{C_{arm}} & 0 & 0 & \frac{\frac{n_{u0}(t)}{2}-(G_v Z_L+G_c)(i_{c0}(t)+\frac{i_{g0}(t)}{2})}{C_{arm}} \\ \frac{n_{l0}(t)-G_{cc}\left(i_{c0}(t)-\frac{i_{g0}(t)}{2}\right)}{C_{arm}} & 0 & 0 & \frac{-\frac{n_{l0}(t)}{2}+(G_v Z_L+G_c)\left(i_{c0}(t)-\frac{i_{g0}(t)}{2}\right)}{C_{arm}} \\ \frac{G_{cc}\left(v_{cu0}^{\Sigma}(t)-v_{cl0}^{\Sigma}(t)\right)}{L} & -\frac{n_{u0}(t)}{L} & \frac{n_{l0}(t)}{L} & -\frac{2Z_L+R}{L} + \frac{(G_v Z_L+G_c)(v_{cu0}^{\Sigma}(t)+v_{cl0}^{\Sigma}(t))}{L} \end{bmatrix} \tag{102}$$

$$B_p(t) = \begin{bmatrix} \frac{G_v(v_{cu0}^{\Sigma}(t) - v_{cl0}^{\Sigma}(t))}{2L} \\ -\frac{G_v(i_{c0}(t) + \frac{i_{g0}(t)}{2})}{C_{arm}} \\ \frac{G_v\left(i_{c0}(t) - \frac{i_{g0}(t)}{2}\right)}{C_{arm}} \\ -\frac{2}{L} + \frac{G_v\left(i_{c0}(t) - \frac{i_{g0}(t)}{2}\right)}{L} \end{bmatrix} \tag{103}$$

Applying HSS modelling method as discussed in Section 3.1 to the small-signal state-space model shown in (99)-(103), the HSS model of the MMC with full controllers can be expressed in the form of (16) where the expression of $\mathbb{X}$, $\mathbb{U}$, $\mathbb{A}$, $\mathbb{B}$, $\mathbb{Q}$ are showed as (17)-(21) in which the elements X_h, U_h, A_h, B_h are the corresponding h-th Fourier coefficients of $X(t), U(t), A(t), B(t)$ as shown in (104)-(110), respectively.

$$A_0 = \begin{bmatrix} \frac{G_{cc}\left(v_{cu0}^{\Sigma}+v_{cl0}^{\Sigma}\right)}{2L} - \frac{R}{L} & -\frac{1}{4L} & -\frac{1}{4L} & \frac{(G_vZ_L+G_c)(v_{cu0}^{\Sigma}-v_{cl0}^{\Sigma})}{2L} \\ \frac{\frac{1}{2}-G_{cc}\left(i_{c0}+\frac{i_{g0}}{2}\right)}{C_{arm}} & 0 & 0 & \frac{\frac{1}{4}-(G_vZ_L+G_c)(i_{c0}+\frac{i_{g0}}{2})}{C_{arm}} \\ \frac{\frac{1}{2}-G_{cc}\left(i_{c0}-\frac{i_{g0}}{2}\right)}{C_{arm}} & 0 & 0 & \frac{-\frac{1}{4}+(G_vZ_L+G_c)\left(i_{c0}-\frac{i_{g0}}{2}\right)}{C_{arm}} \\ \frac{G_{cc}\left(v_{cu0}^{\Sigma}-v_{cl0}^{\Sigma}\right)}{L} & -\frac{1}{2L} & \frac{1}{2L} & -\frac{2Z_L+R}{L}+\frac{(G_vZ_L+G_c)(v_{cu0}^{\Sigma}+v_{cl0}^{\Sigma})}{L} \end{bmatrix} \tag{104}$$

$$A_{\pm1} = \begin{bmatrix} \frac{G_{cc}\left(v_{cu\pm1}^{\Sigma}+v_{cl\pm1}^{\Sigma}\right)}{4L} & \frac{m_1}{8L}e^{\pm j\theta_{m1}} & -\frac{m_1}{8L}e^{\pm j\theta_{m1}} & \frac{(G_vZ_L+G_c)(v_{cu\pm1}^{\Sigma}-v_{cl\pm1}^{\Sigma})}{4L} \\ -\frac{m_1e^{\pm j\theta_{m1}}}{4C_{arm}} - \frac{G_{cc}\left(i_{c\pm1}-\frac{i_{g\pm1}}{2}\right)}{2C_{arm}} & 0 & 0 & \frac{-\frac{m_1}{4}e^{\pm j\theta_{m1}}-(G_vZ_L+G_c)(i_{c\pm1}+\frac{i_{g\pm1}}{2})}{2C_{arm}} \\ \frac{m_1e^{\pm j\theta_{m1}}}{4C_{arm}} - \frac{G_{cc}\left(i_{c\pm1}-\frac{i_{g\pm1}}{2}\right)}{2C_{arm}} & 0 & 0 & \frac{-\frac{m_1}{4}e^{\pm j\theta_{m1}}+(G_vZ_L+G_c)\left(i_{c\pm1}-\frac{i_{g\pm1}}{2}\right)}{2C_{arm}} \\ \frac{G_{cc}\left(v_{cu\pm1}^{\Sigma}-v_{cl\pm1}^{\Sigma}\right)}{2L} & \frac{m_1}{4L}e^{\pm j\theta_{m1}} & \frac{m_1}{4L}e^{\pm j\theta_{m1}} & \frac{(G_vZ_L+G_c)(v_{cu\pm1}^{\Sigma}+v_{cl\pm1}^{\Sigma})}{2L} \end{bmatrix} \tag{105}$$

$$A_{\pm2} = \begin{bmatrix} \frac{G_{cc}\left(v_{cu\pm2}^{\Sigma}+v_{cl\pm2}^{\Sigma}\right)}{4L} & \frac{m_2}{8L}e^{\pm j\theta_{m2}} & -\frac{m_2}{8L}e^{\pm j\theta_{m2}} & \frac{(G_vZ_L+G_c)(v_{cu\pm2}^{\Sigma}-v_{cl\pm2}^{\Sigma})}{4L} \\ -\frac{m_2e^{\pm j\theta_{m2}}}{4C_{arm}} - \frac{G_{cc}\left(i_{c\pm2}-\frac{i_{g\pm2}}{2}\right)}{2C_{arm}} & 0 & 0 & \frac{-\frac{m_2}{4}e^{\pm j\theta_{m2}}-(G_vZ_L+G_c)(i_{c\pm2}+\frac{i_{g\pm2}}{2})}{2C_{arm}} \\ \frac{m_2e^{\pm j\theta_{m2}}}{4C_{arm}} - \frac{G_{cc}\left(i_{c\pm2}-\frac{i_{g\pm2}}{2}\right)}{2C_{arm}} & 0 & 0 & \frac{-\frac{m_2}{4}e^{\pm j\theta_{m2}}+(G_vZ_L+G_c)\left(i_{c\pm2}-\frac{i_{g\pm2}}{2}\right)}{2C_{arm}} \\ \frac{G_{cc}\left(v_{cu\pm2}^{\Sigma}-v_{cl\pm2}^{\Sigma}\right)}{2L} & \frac{m_2}{4L}e^{\pm j\theta_{m2}} & \frac{m_2}{4L}e^{\pm j\theta_{m2}} & \frac{(G_vZ_L+G_c)(v_{cu\pm2}^{\Sigma}+v_{cl\pm2}^{\Sigma})}{2L} \end{bmatrix} \tag{106}$$

$$A_{\pm h} = \begin{bmatrix} \frac{G_{cc}\left(v_{cu\pm h}^{\Sigma}+v_{cl\pm h}^{\Sigma}\right)}{4L} & 0 & 0 & \frac{(G_vZ_L+G_c)(v_{cu\pm h}^{\Sigma}-v_{cl\pm h}^{\Sigma})}{4L} \\ -\frac{G_{cc}\left(i_{c\pm h}(t)-\frac{i_{g\pm h}(t)}{2}\right)}{2C_{arm}} & 0 & 0 & \frac{-(G_vZ_L+G_c)(i_{c\pm h}+\frac{i_{g\pm h}}{2})}{2C_{arm}} \\ -\frac{G_{cc}\left(i_{c\pm h}-\frac{i_{g\pm h}}{2}\right)}{2C_{arm}} & 0 & 0 & \frac{(G_vZ_L+G_c)\left(i_{c\pm h}-\frac{i_{g\pm h}}{2}\right)}{2C_{arm}} \\ \frac{G_{cc}\left(v_{cu\pm h}^{\Sigma}-v_{cl\pm h}^{\Sigma}\right)}{2L} & 0 & 0 & \frac{(G_vZ_L+G_c)(v_{cu\pm h}^{\Sigma}+v_{cl\pm h}^{\Sigma})}{2L} \end{bmatrix}, (\,h \geq 3) \tag{107}$$

$$B_0 = \begin{bmatrix} \frac{G_v(v_{cu0}^{\Sigma} - v_{cl0}^{\Sigma})}{2L} \\ -\frac{G_v(i_{c0} + \frac{i_{g0}}{2})}{C_{arm}} \\ \frac{G_v\left(i_{c0} - \frac{i_{g0}}{2}\right)}{C_{arm}} \\ -\frac{2}{L} + \frac{G_v\left(i_{c0} - \frac{i_{g0}}{2}\right)}{L} \end{bmatrix} \tag{108}$$

$$B_{\pm 1} = \begin{bmatrix} \frac{G_v(v_{cu\pm 1}^{\Sigma} - v_{cl\pm 1}^{\Sigma})}{2L} \\ -\frac{G_v\left(i_{c\pm 1} + \frac{i_{g\pm 1}}{2}\right)}{C_{arm}} \\ \frac{G_v\left(i_{c\pm 1} - \frac{i_{g\pm 1}}{2}\right)}{C_{arm}} \\ \frac{G_v\left(i_{c\pm 1} - \frac{i_{g\pm 1}}{2}\right)}{L} \end{bmatrix} \tag{109}$$

$$B_{\pm h} = \begin{bmatrix} \frac{G_v(v_{cu\pm h}^{\Sigma} - v_{cl\pm h}^{\Sigma})}{2L} \\ -\frac{G_v\left(i_{c\pm h} + \frac{i_{g\pm h}}{2}\right)}{C_{arm}} \\ \frac{G_v\left(i_{c\pm h} - \frac{i_{g\pm h}}{2}\right)}{C_{arm}} \\ \frac{G_v\left(i_{c\pm h} - \frac{i_{g\pm h}}{2}\right)}{L} \end{bmatrix}, (h \geq 2) \tag{110}$$

4.3.2 Impedance model validation of the MMC with CCC

In this part, the analytic model of the MMC system includes CCC controller is validated against the RTDS, PSCAD and Simulink time-domain model. The AC-side impedance of time-domain models is measured using the same way as described in Section 3.3. The harmonic order h of the analytical model is selected as 0, 1, and 2. As shown in Figure 11, the analytical impedance has a good agreement with the measured results in the simulation, which validates the analytical MMC impedance model. Moreover, it is worth

noting that the high order harmonic components are well suppressed by CCSC so the analytical model with h=2 is sufficiently accurate.

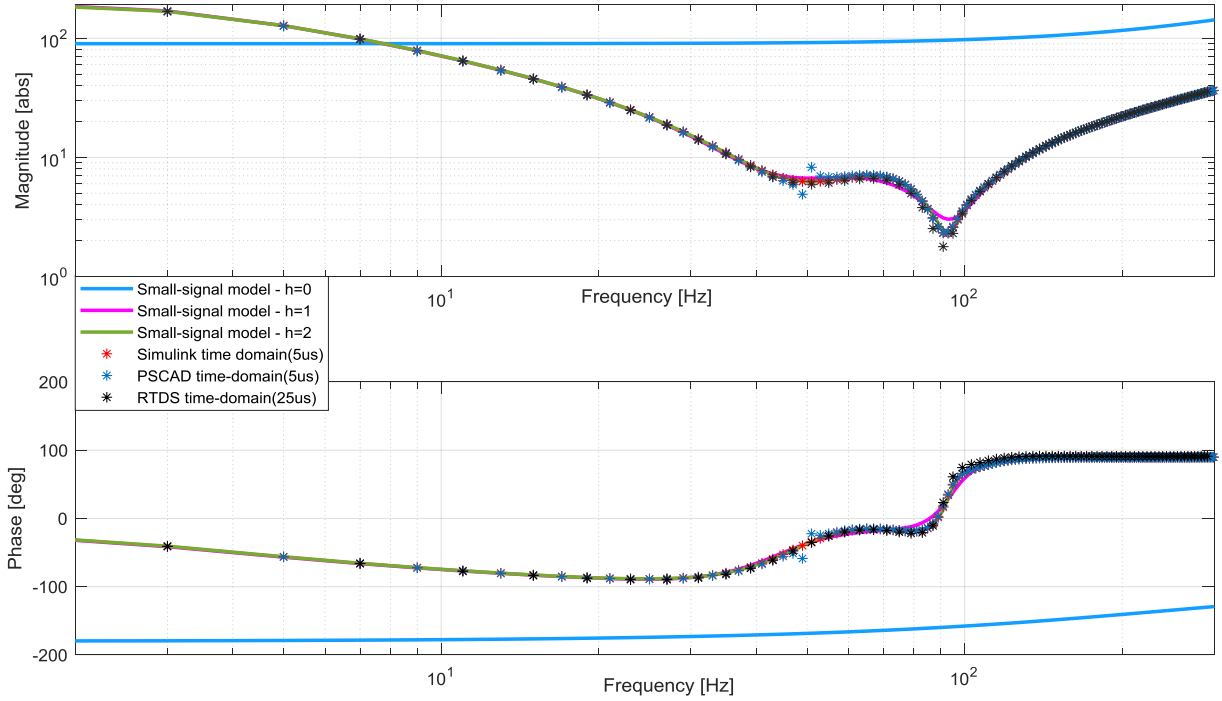

Figure 11: Analytical and simulation measured impedances of the MMC with CCSC

4.3.3 Impedance model validation of the MMC with full control

Figure 12 shows the comparison between the analytical and simulation results of the measured AC-side small-signal impedance of the MMC with CCC and *dq* current loop control. The AC-side impedance of the time-domain models is measured using the same way as described in Section 3.3. The harmonic orders h of the analytical model are selected as 1 and 2. As can be seen, the analytical impedances agree well with the measured results in the time-domain simulation, which validates the analytical MMC impedance model. When the harmonic order $h = 1$, the analytical impedance model is actually accurate enough since the magnitude and phase of the model overlap with that of the time-domain measured impedance respectively. Comparing the measured impedance plots of PSCAD with different simulation time-steps, it can be indicated that 25us solution time-step is also sufficiently accurate for impedance measuring of time-domain MMC model with CCSC and current loop controllers. This is largely due to the fact that once the full controllers are implemented, the interactions between different harmonics are reduced and thus the requirement on accuracy of the time-domain simulation is also lowered.

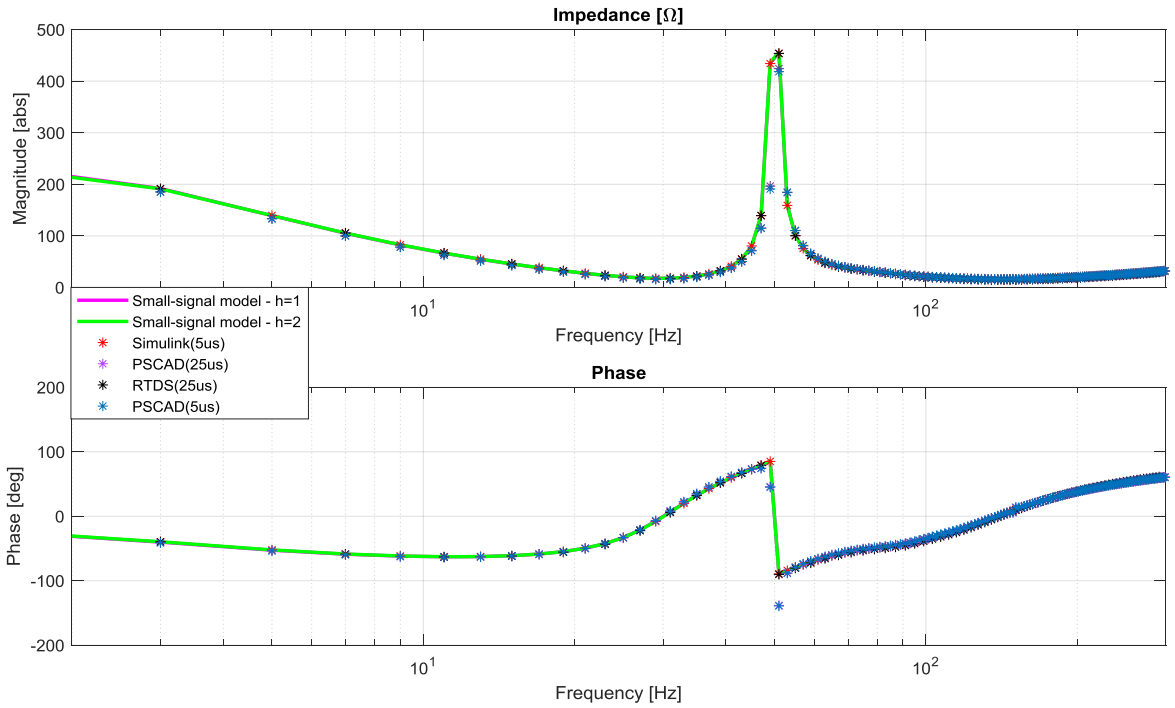

Figure 12: Analytical and simulation measured impedances of the MMC with full control

5 Discussion and further work

Significant amount of research work have already been carried out in developing adequate modelling methods and models for MMC for stability study. During the course of the development work, it was discovered that there still exist noticeable gaps between the knowledge in the open literature and adequate modelling method that can be used for assessing system stability with multiple MMCs in a network.

The existing modelling methods are based on the single-phase concept which is considered as an "easy" approach due to the unique configuration of a MMC. As in a MMC, the three internal legs and the DC link form an equivalent 3-phase 4-wire system, so they can be considered as 3 independent single-phase. However, for the external 3-phase AC terminals, it becomes a 3-phase 4-wire system only if a common AC and DC grounding point exist. Thus, the single-phase modelling approach is valid only when a common AC and DC grounding point exist, and both the external AC system and phase legs behave as 3 single-phase systems. However, in most practical systems, there is no common AC and DC grounding point and thus, the single-phase modelling approach is not entirely valid. To address this issue, work is currently being carried out to model the system in stationary α, β, and zero frame in which the system is combined of internal legs (with zero sequence) and external AC terminals (without zero sequence). The full results will be reported in the second report together with the study of AC network impedance model.

In order to ensure additional control loops, e.g., PLL, AC voltage control, power control etc., can be easily incorporated into the impedance model, an approach which uses modular modelling concept is also being developed. Such approach will allow modifications on control system to be easily implemented into the small signal models without the need to recalculate the various state matrix.

6 Conclusion

This report has described the impedance modelling and validation of the MMC converter. The fundaments on impedance based converter modelling have been introduced. The detailed mathematical expressions for harmonic state space (HSS) modelling for MMC have been derived considering the integration of circulating current control and da based AC current control. The small signal impedances obtained from the developed analytical model have been validated using time-domain models. It has shown that:

- For open loop MMC system, it is important that higher order harmonics (e.g. $h \gg 4$) are considered in order to accurately model the impedance behaviour of the MMC. This is due to the fact that for open loop MMC system, there exist strong coupling among the harmonics and high harmonic order is thus required to accurately represent the system dynamics in the small signal model.
- Once the circulating current controller and AC current controller are included, due to the largely eliminated circulating current, the harmonic interaction of MMC is reduced, and the results show that impedance model with h=2 provides sufficient accuracy.
- When considering small signal impedance model, simulation time step in the time-domain model can impact on the obtained impedance especially when there exist multiple harmonic interactions. This is especially true for RTDS model due to the use of relatively larger RTDS time steps.
- However, it has been observed that once the full sets of control system are added, the harmonic coupling of the MMC system is reduced. Consequently, time domain simulation with larger time step, as in RTDS cases, produces almost identical results as those with small time step simulations. This imply the full system impedance model extracted from RTDS models should be adequate for the stability study.

The developed small signal MMC model will be combined with the impedance of a representative AC network model (Task 2) for system stability assessment based on Nyquist stability criterion (Task 3).

7 References

[1] M. Liserre, R. Theodorescu, and F. Blaabjerg, “Stability of photovoltaic and wind turbine grid-connected inverters for a large set of grid impedance values,” *IEEE Trans. Power Electron.*, vol. 21, no. 1, pp. 263–272, Jan. 2006.

[2] J. Sun, “Impedance-based stability criterion for grid-connected inverters”, *IEEE Trans. Power Electron.*, vol. 26, no. 11, pp. 3075–3078, Nov. 2011.

[3] J. Lyu, M. Molinas, and X. Cai, “Harmonic State Space Modeling of a Three-Phase Modular Multilevel Converter”, *2018 IEEE Int. Power Electron. Appl. Conf. Expo.*, no. June, pp. 650–655, 2018.

[4] N. M. Wereley and S. R. Hall, "Linear Time Periodic Systems: Transfer Function, Poles, Transmission Zeroes and Directional Properties", *1991 American Control Conference*, Boston, MA, USA, 1991, pp. 1179-1184.

[5] TR on Modular Multilevel Voltage Source Converter: Fundamentals and Synthesis of Different Models, *Strathclyde-UK National HVDC Centre collaborative research project*, TR ref. USTRATH-HVDC Centre-P1-001, April 2018.